Polyelectrolyte complex coacervation: Effects of concentration asymmetry

Pengfei Zhang, Nayef M. Alsaifi, Jianzhong Wu, and Zhen-Gang Wang

Citation: The Journal of Chemical Physics **149**, 163303 (2018); doi: 10.1063/1.5028524
View online: https://doi.org/10.1063/1.5028524
View Table of Contents: http://aip.scitation.org/toc/jcp/149/16
Published by the American Institute of Physics

Polyelectrolyte complex coacervation: Effects of concentration asymmetry

Pengfei Zhang,[1] Nayef M. Alsaifi,[1,2] Jianzhong Wu,[3] and Zhen-Gang Wang[1,a)]
[1]*Division of Chemistry and Chemical Engineering, California Institute of Technology, Pasadena, California 91125, USA*
[2]*Chemical Engineering Department, King Fahd University of Petroleum and Minerals, Dhahran, Saudi Arabia*
[3]*Department of Chemical and Environmental Engineering, University of California, Riverside, California 92521, USA*

(Received 11 March 2018; accepted 23 April 2018; published online 6 July 2018)

Using a simple liquid-state theory, we study the phase behaviors of *concentration-asymmetric* mixtures of polycation and polyanion solutions. We construct a three-dimensional (3D) phase diagram in terms of the concentrations of the three independent charged components: polycation, polyanion, and small cation ($\rho_{p+}-\rho_{p-}-\rho_{+}$), for a given Bjerrum length. This phase diagram yields rich and complex phase-separation scenarios. To illustrate, we sequentially examine the following three systems that are directly relevant to experiments: a symmetric mixture, an asymmetric mixture with one type of small ions, and an asymmetric mixture with both types of small ions. We re-express the information in the 3D phase diagram using three experimentally more easily controllable parameters—the asymmetry factor r, the initial extra-salt concentration $\rho_{s,0}$, and the initial polyelectrolyte (PE) concentration $\rho_{p,0}$ of both solutions prior to mixing. We construct three reduced phase diagrams in the $\rho_{p,0}-r$, $r-\rho_{s,0}$, and $\rho_{s,0}-\rho_{p,0}$ planes, respectively, and examine the evolution of the volume fraction of the coexisting phases, concentration of the PE and small-ion species in each phase, and the Galvani potential Ψ_G, as functions of these experimental controlling parameters. We rationalize our findings in terms of the key thermodynamic factors, namely, the translational entropy of the small ions, the electrostatic correlation energy, and the requirement for charge neutrality. *Published by AIP Publishing.* https://doi.org/10.1063/1.5028524

I. INTRODUCTION

Many biological systems and technological applications involve complexation between oppositely charged macro-ions such as colloidal particles, polyelectrolytes (PEs), and ionic surfactants. Examples include PE multilayer films,[1,2] microcapsules in drug delivery,[3,4] and underwater bioadhesives such as mussels and sandcastle worms.[5–7] Theoretical understanding of the phase behaviors of such systems is one of the key steps for improving the physical properties of the charge complex in technological applications. As a prototypical example, aqueous solutions of polycation and polyanion mixtures have been studied extensively.[8–14] For such mixtures, under appropriate conditions, electrostatic attraction between oppositely charged PE chains can cause the system to undergo a macroscopic phase-separation into a dilute (in PE) supernatant phase and a denser PE-rich phase. When the PE-rich phase is in the liquid state, it is called "coacervate" and the liquid-liquid phase-separation is referred to as complex coacervation; when the PE-rich phase is in the solid state, it usually precipitates out from the solution and the phenomenon is referred to as complex precipitation. In the present study, we do not distinguish between the coacervate and precipitate states since the mechanism of transition between the two is currently unknown; we will therefore use the general term "PE-rich phase" to describe the more concentrated phase and use the term "PE-poor phase" to denote the dilute supernatant phase.

Theoretical investigation on the phase behavior of oppositely charged PE mixture solutions was pioneered by Voorn and Overbeek[15,16] about six decades ago. The free energy in the Voorn-Overbeek (VO) theory combines the Flory-Huggins mixing entropy with the Debye-Hückel correlation energy.[17] The VO theory is able to qualitatively capture phase behaviors of symmetric polycation and polyanion mixtures[15,16,18–21] and is still used in recent studies.[22,23] However, since the DH correlation energy[17] is only valid for simple ionic solutions in the dilute limit, several advanced theories[24–37] have been proposed to incorporate the effects of chain connectivity, ion-paring, and counterion release; we refer readers to two recent reviews on some of these developments.[12,13] In spite of the large number of theoretical studies, most previous publications focus on symmetric mixtures,[16,25–27,30–36] in which polycations and polyanions are assumed to have the same chain length, flexibility, charge fraction, and concentration. Experimentally, *asymmetry* in one or more of these parameters is nearly unavoidable.[22,38–45] However, apart from a few theoretical or simulation studies[20,28,37,46–50] that have examined some specific asymmetry effects in these parameters, a comprehensive picture of how asymmetry affects the phase behavior is still lacking.

Consider the *simplest* asymmetric mixture: suppose initially, we have a polycation solution and a symmetric

a)Electronic mail: zgw@caltech.edu

polyanion solution both in the homogeneous phase and having the *same* parameters (including the chain length, PE concentration, charge fraction, and salt concentration). The volume of the polycation solution is V_1 and that of the polyanion solution is V_2. We wish to determine the final state of the system when these two solutions are mixed together; see Fig. 1. The asymmetry here thus refers to the asymmetry in the overall concentrations between polycations and polyanions in the mixture. This concentration-asymmetry is more conveniently represented by the volume difference between the two initial solutions; we thus define an asymmetry factor $r \equiv (V_1 - V_2)/(V_1 + V_2)$ such that $r = 0$ corresponds to a symmetric mixture, while $r = -1$ (or 1) corresponds to a pure polyanion (or polycation) solution. Even for this simplest asymmetric mixture, the phase behavior is still rather complex. For instance, a mean-field RPA analysis predicted that there can be a variety of mesoscopic structures such as spherical, cylindrical, or lamellar complexes for weakly asymmetric solutions.[46] We will not be concerned with such *mesoscopic* complex structures in this work. Instead, we focus on the general *macroscopic* phase behavior by studying the global phase diagram and exploring its experimental implications.

We note that some aspects of the phase behavior of concentration-asymmetric mixtures have been studied by the VO theory,[20] and several interesting phenomena have been obtained. For example, phase-separation can be inhibited when the mixture is sufficiently asymmetric. However, a *systematic* investigation on the global features of the phase diagram and the influence of various parameters (such as the asymmetry factor r, the initial PE concentration, and the extra-salt concentration) is still missing. Moreover, since the VO theory completely neglects chain connectivity in the treatment of the electrostatic correlation, it is unable to capture some interesting experimental phenomena, such as the closed-loop phase diagram for a single species PE solution with

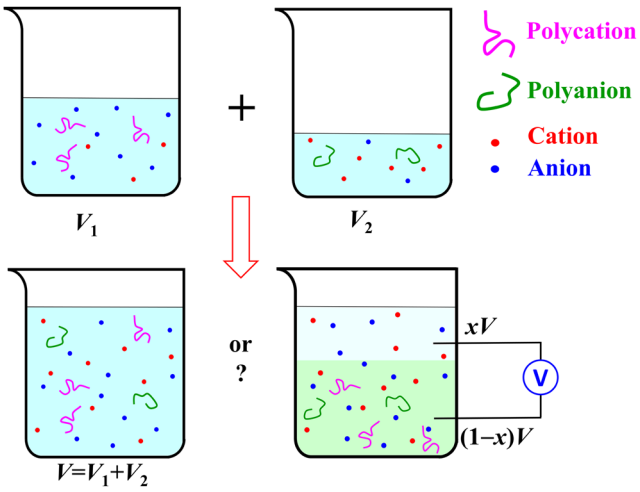

FIG. 1. Schematic for the phase behavior of a concentration–asymmetric polycation and polyanion mixture. In this work, we consider the concentration asymmetry to be controlled by the different volumes V_1 and V_2 for the initial polycation and polyanion solutions, respectively, which are otherwise completely symmetric (i.e., the same chain length, charge fraction, and concentration for each component). x and $1 - x$ refer to the volume fractions of the PE-poor phase and the PE-rich phase, respectively.

monovalent salt.[51,52] In view of the success of a simple liquid-state (LS) theory[53,54] in describing the phase behavior of a PE solution with simple salt, as demonstrated in our recent work,[52] here we adopt the same theory to investigate the phase behavior of concentration-asymmetric mixtures described above.

Like many analytical theories for bulk solutions, the LS theory is unable to accurately describe the thermodynamics when the PE concentration is low, both because it neglects the chain connectivity correlations beyond the adjacent monomers along the chain backbone and because it does not account for strong correlation effects such as the polycation-polyanion pair formation[32] and counterion condensation in the supernatant phase. Nevertheless, we adopt it here in this work because it is a more refined theory than the VO theory in that it captures some leading order corrections due to chain connectivity and electrostatic correlations beyond Debye-Hückel, and it has an analytical expression for the free energy, which greatly facilitates the construction of the multidimensional phase diagrams. This last feature is particularly attractive since our main purpose here is to obtain a global picture of the phase behavior of the concentration-asymmetric mixtures and to explore possible experimental implications. For the questions of interest in this work, we believe that the quantitative inaccuracy in its treatment of the dilute phase does not alter the qualitative physics we wish to elucidate.

Using this LS theory, we systematically study phase behaviors of a polycation and polyanion mixture. In particular, we construct the three-dimensional (3D) polycation–polyanion–cation concentration phase diagram at a fixed Bjerrum length l_B. This 3D phase diagram in principle contains the complete information on the phase behavior at the specified l_B and yields rich and complex phase-separation scenarios. To illustrate, we examine the following three systems sequentially: 1. a symmetric polycation and polyanion mixture, 2. an asymmetric polycation and polyanion mixture with one type of small ions, and 3. an asymmetric polycation and polyanion mixture with both types of small ions. For the first system, the LS theory predicts that, except for mixtures with very low overall salt concentration, the concentration of small ions is slightly higher in the PE-poor phase, contrary to the VO results. The second system can be interpreted as an asymmetric polyacid and polybase mixture; we thus examine the titration behavior of a polyacid with a polybase. One simple experimental setup for the third system is already depicted schematically in Fig. 1. For the third system, there are three parameters—the asymmetry factor r, the initial PE concentrations $\rho_{p,0}$, and the extra-salt concentrations $\rho_{s,0}$—that govern the phase behaviors. We thus investigate their effects in turn.

The paper is organized as follows. In Sec. II, we briefly recapitulate the key features in the model and the key equations in the LS theory. In Sec. III, we discuss the 3D phase diagram for the concentration-asymmetric polycation and polyanion mixture and explore the different phase-separation scenarios for the three systems specified above. In Sec. IV, we summarize the key results and present a brief outlook along with some open questions.

II. THEORETICAL FORMULATION

A. Liquid-state theory

The theoretical model and LS theory[53,54] used in this study are similar to those reported in our previous work.[52] Here, for completeness, we briefly recapitulate the key ingredients of the model and the key equations.

We consider a mixture of polycation and polyanion solutions with small ions. For simplicity, we assume that the cations and anions from the salts are identical to the counterions of the polyanions and polycations, respectively. We thus have a total of four charged species—polycation, polyanion, small cation, and small anion; henceforth we will refer to the small cation and small anion simply as cation and anion, respectively. We use the primitive model[17] to describe the system: the solvent is treated as a dielectric continuum with a dielectric constant ϵ_r, the cations (anions) are modeled as positively (negatively) charged hard spheres with diameter σ_+ (σ_-), and a polycation (polyanion) chain is assumed to consist of N_{p+} (N_{p-}) tangentially connected positively (negatively) charged hard spheres with diameter σ_{p+} (σ_{p-}). Denoting the concentration and the valency of component i as ρ_i and z_i, respectively ($i = p+, p-, +, -$), global charge neutrality requires that $\sum_i \rho_i z_i = 0$, where obviously the density and valency for the PE chains refer to those of the monomers. In order to highlight the effect of electrostatic interaction, we assume no other interactions besides the electrostatic interaction and the hard-core excluded volume repulsion.

We write the Helmholtz free energy density as a sum of an ideal part and an excess part, $f = f^{\mathrm{id}} + f^{\mathrm{ex}}$. The ideal part describes the translational degrees of freedom for all explicit components and is known exactly,

$$\beta f^{\mathrm{id}} = \sum_{j=p\pm} \frac{\rho_j}{N_j}\left[\ln\left(\frac{\rho_j}{N_j}\Lambda_j^3\right) - 1\right] + \sum_{i=\pm} \rho_i(\ln \rho_i\Lambda_i^3 - 1), \quad (1)$$

where $\beta \equiv 1/k_BT$ with k_B being the Boltzmann constant and T being the absolute temperature, Λ_j and Λ_i are length scales arising from integration over the momentum degrees of freedom, which have no consequence for the phase behavior.

In the framework of Wertheim's first-order thermodynamic perturbation (TPT1) theory,[55–57] the excess Helmholtz free energy density can be decomposed into three terms $f^{\mathrm{ex}} = f_{\mathrm{hs}} + f_{\mathrm{el}} + f_{\mathrm{ch}}$, where the first term represents the hard-core excluded volume repulsion of uncharged hard spheres, the second term describes the electrostatic correlation correction for disconnected charged hard spheres, and the last term accounts for the free energy change in connecting charged hard spheres into chains. The excluded volume repulsion of uncharged hard spheres can be accurately described by the Boublík-Mansoori-Carnahan-Starling-Leland (BMCSL) excess free energy density[58,59]

$$\beta f_{\mathrm{hs}} = -n_0\ln(1-\eta) + \frac{n_1 n_2}{1-\eta} + \frac{n_2^3}{36\pi\eta^3}\left[\eta\ln(1-\eta) + \frac{\eta^2}{(1-\eta)^2}\right], \quad (2)$$

with $n_0 \equiv \sum_i \rho_i$, $n_1 \equiv (\sum_i \rho_i\sigma_i)/2$, $n_2 \equiv \pi\sum_i \rho_i\sigma_i^2$, and $\eta \equiv (\pi/6)\sum_i \rho_i\sigma_i^3$. When the diameters for all hard spheres are equal, Eq. (2) reduces to the well-known Carnahan-Starling excess free energy density $\beta f_{\mathrm{hs}} = 6\eta^2(4-3\eta)/[\pi\sigma^3(1-\eta)^2]$.[60,61]

The electrostatic correlation for charged hard spheres can be taken into account by solving the Ornstein-Zernike equation under various closures such as hypernetted chain (HNC) approximation[61] and mean spherical approximation (MSA).[62–65] Here we choose MSA both because it affords a simple analytical expression and because it yields qualitatively or even quantitatively correct results at low to intermediate ionic concentrations for a wide range of electrostatic correlation strength. Under the MSA, the excess free energy density due to electrostatic correlation is[65]

$$\beta f_{\mathrm{el}} = -l_B\sum_i \frac{\rho_i z_i}{1+\Gamma\sigma_i}\left[\Gamma z_i + \frac{\pi P_n\sigma_i}{2(1-\eta)}\right] + \frac{\Gamma^3}{3\pi}, \quad (3)$$

where the Bjerrum length $l_B \equiv \beta e^2/4\pi\epsilon_0\epsilon_r$, with e being the elementary charge and ϵ_0 being the vacuum permittivity, characterizes the length at which the electrostatic interaction between two unit charges in the dielectric continuum is equal to the thermal energy k_BT; Γ and P_n are, respectively, the screening parameter and the size asymmetry factor, and their respective expressions can be found in Ref. 52. For the equal-size systems, invoking charge neutrality, one gets $P_n = 0$ and Eq. (3) reduces to $\beta f_{\mathrm{el}}^{\mathrm{ex}} = -\Gamma^3(2/3+\Gamma\sigma)/\pi$,[62,63] where Γ satisfies $\Gamma(1+\Gamma\sigma) = \kappa/2$ with $\kappa \equiv \sqrt{4\pi l_B\sum_i \rho_i z_i^2}$ being the inverse of the Debye screening length.[17] In the dilute limit $\rho_i \to 0$, $2\Gamma \to \kappa$ and $\beta f_{\mathrm{el}} \to -\kappa^3/12\pi$; we thus recover the DH electrostatic correlation free energy.

As a simple method to treat the excess Helmholtz free energy due to chain connectivity, the first-order thermodynamic perturbation theory (TPT1) was originally proposed by Wertheim for neutral hard-sphere chain systems[55–57] and later generalized by Jiang *et al.* to PE solutions.[53,54] TPT1 accounts for the correlation effect due to chain connectivity only at the pair level for the connected spheres; the excess free energy contribution is

$$\beta f_{\mathrm{ch}}^{\mathrm{ex}} = \sum_{i=p\pm} \rho_i\left(\frac{1}{N_i} - 1\right)\ln\left[g_i(\sigma_i)\exp\left(\frac{l_B z_i^2}{\sigma_i}\right)\right], \quad (4)$$

where $g_i(\sigma_i)$ is the contact value of the radial distribution function of the collection of disconnected charged hard-spheres comprising the PE chains. The MSA theory provides a simple analytical form for $g_i(\sigma_i)$, i.e.,

$$g_i^{\mathrm{MSA}}(\sigma_i) = \frac{1}{1-\eta} + \frac{n_2\sigma_i}{4(1-\eta)^2} - \frac{l_B}{\sigma_i(1+\Gamma\sigma_i)^2}\left[z_i - \frac{\pi P_n\sigma_i^2}{2(1-\eta)}\right]^2, \quad (5)$$

where the sum of the first and the second terms on the right-hand side is the contact value of the monomer-monomer radial distribution function for disconnected neutral hard spheres from the Percus-Yevick equation,[61,68] denoted as $g_i^{\mathrm{HS}}(\sigma_i)$ hereafter, and the last term is due to the electrostatic correlation. For larger l_B, however, $g_i^{\mathrm{MSA}}(\sigma_i)$ can become negative, which is unphysical. This unphysical feature can be avoided

by making the exponential approximation,[66] which has been shown to give more accurate predictions in their comparison with Monte Carlo simulation results.[66,67] In the exponential approximation, we have

$$g_i^{\mathrm{EXP}}(\sigma_i) = g_i^{\mathrm{HS}}(\sigma_i)\exp\left[g_i^{\mathrm{MSA}}(\sigma_i) - g_i^{\mathrm{HS}}(\sigma_i)\right] = \left[\frac{1}{1-\eta} + \frac{n_2\sigma_i}{4(1-\eta)^2}\right] \times \exp\left\{-\frac{l_B}{\sigma_i(1+\Gamma\sigma_i)^2}\left[z_i - \frac{\pi P_n \sigma_i^2}{2(1-\eta)}\right]^2\right\}. \quad (6)$$

Substituting $g_i^{\mathrm{EXP}}(\sigma_i)$ into Eq. (4), we have the excess free energy density due to chain connectivity as

$$\beta f_{\mathrm{ch}} = \sum_{i=p\pm}\rho_i\left(\frac{1}{N_i} - 1\right)\left\{\ln\left[\frac{1}{1-\eta} + \frac{n_2\sigma_i}{4(1-\eta)^2}\right] + \frac{l_B z_i^2}{\sigma_i} - \frac{l_B}{\sigma_i(1+\Gamma\sigma_i)^2}\left[z_i - \frac{\pi P_n\sigma_i^2}{2(1-\eta)}\right]^2\right\}. \quad (7)$$

B. Construction of phase diagram

From the Helmholtz free energy density f, we compute the chemical potential of each component as $\mu_i \equiv \partial f/\partial\rho_i|_{\rho_{j\neq i}}$ and the (osmotic) pressure as $P = \sum_i \rho_i\mu_i - f$. Note that for the PE, the chemical potential here refers to that of the monomer, i.e., the chemical potential of the PE chains divided by the chain length N. At a given l_B and N, phase equilibrium between the PE-poor phase (denoted as phase I) and its coexisting PE-rich phase (denoted as phase II) is determined by equality of the (osmotic) pressure $P^{\mathrm{I}} = P^{\mathrm{II}}$ and equality of the *electrochemical* potential for all components $\mu_i^{\mathrm{I}} = \mu_i^{\mathrm{II}} + ez_i\Psi_G$, where the Galvani potential Ψ_G denotes the electric potential difference between the PE-rich phase and its coexisting PE-poor phase[52,69] and arises from the asymmetry between oppositely charged components in each of the coexisting phases. For the concentration-*asymmetric* mixture of oppositely charged PE solutions, there are four explicit charged components—polycation, polyanion, cation, and anion; by invoking charge neutrality, only three of them are independent and we hereafter choose them as polycation, polyanion, and cation without loss of generality. The Gibbs phase rule implies that there are two degrees of freedom for such mixtures with two coexisting phases at a given l_B. Therefore, the coexisting concentrations form a binodal surface in the three-dimensional ρ_{p+}–ρ_{p-}–ρ_+ phase diagram, as elaborated later. The analysis based on the Gibbs phase rule and the numerical details are presented in Sec. I A of the supplementary material. In addition, we present an alternative way to construct the phase diagram in Sec. I B of the supplementary material.

To reduce the huge parameter space $\{\rho_i, N_i, z_i, \sigma_i, l_B\}$ ($i = p\pm, \pm$), in the following, we assume that all charged spheres have the same diameter σ and are monovalent ($z_{p+} = z_+ = -z_{p-} = -z_- = 1$); both PE chains have the same chain length ($N_{p+} = N_{p-} = N$) and we take $N = 100$ for most cases. For notational simplicity, we define dimensionless quantities—reduced Bjerrum length $\tilde{l}_B \equiv l_B/\sigma$, reduced concentration $\tilde{\rho}_i \equiv \rho_i\sigma^3$, reduced chemical potential $\tilde{\mu} \equiv \beta\mu$, and reduced Galvani potential $\tilde{\Psi}_G \equiv \beta e\Psi_G$. In particular, $\tilde{l}_B$ serves to quantify the strength of the electrostatic interaction, which can be adjusted by changing either the temperature T, the dielectric constant ϵ_r, or the hard-sphere diameter σ. To further simplify the notation, henceforth we drop the tilde $\sim$ sign in these quantities. Most of our calculations are performed using the LS theory; VO calculation is only performed for the symmetric mixture to highlight the importance of chain connectivity contribution to the excess thermodynamic properties.

III. RESULTS AND DISCUSSION

A. 3D phase diagram

As stated earlier, for a general concentration-asymmetric polycation and polyanion mixture at fixed l_B, coexistence between the PE-poor phase with $(\rho_{p+}^{\mathrm{I}}, \rho_{p-}^{\mathrm{I}}, \rho_+^{\mathrm{I}})$ and the PE-rich phase with $(\rho_{p+}^{\mathrm{II}}, \rho_{p-}^{\mathrm{II}}, \rho_+^{\mathrm{II}})$ forms a surface in the 3D ρ_{p+}–ρ_{p-}–ρ_+ phase diagram. Moreover, due to symmetry between oppositely charged components, the binodal surface is symmetric under the exchange $\rho_{p+} \leftrightarrow \rho_{p-}$ and $\rho_+ \leftrightarrow \rho_-$. Therefore, we restrict to the half space with $\rho_{p+} \geq \rho_{p-}$. In Fig. 2, we show several representative curves on the binodal surface at fixed concentration differences between the polycation and polyanion in the PE-rich phase, i.e., $\rho_{p+}^{\mathrm{II}} - \rho_{p-}^{\mathrm{II}} = 0, 0.01, 0.015, 0.02, 0.03, 0.04, 0.05, 0.0623$, respectively, for $l_B = 1.785$ and $N = 100$. (This value of the dimensionless Bjerrum length corresponds to aqueous solutions of PE monomer diameter about 4 Å.) The binodal surface separates the single-phase region (above) from the two-phase region (below). The tie lines, connecting concentrations of the coexisting phases, are shown as the magenta dashes; the red curve denotes the critical curve at which the coexisting phases merge together (i.e., $\rho_i^{\mathrm{I}} = \rho_i^{\mathrm{II}}$). Although not shown here, as l_B increases, the binodal surface moves upwards, indicating broadening of the two-phase region, while with decreasing l_B, the binodal surface shifts downwards and disappears at some Bjerrum length $l_B \approx 0.2$, defined as the critical Bjerrum length $l_{B,c}$ hereafter. We note that a similar binodal surface was constructed, respectively, by using VO theory[10] and by a transition matrix

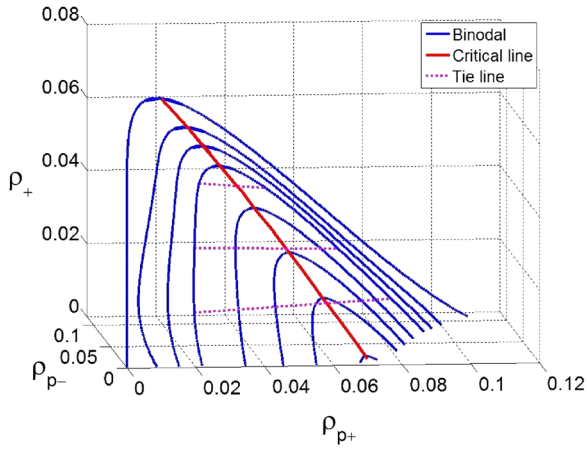

FIG. 2. Phase diagram of a concentration-*asymmetric* polycation and polyanion solution mixture with small ions for $l_B = 1.785$ and $N = 100$. See the main text for details.

TABLE I. Components for the three systems examined.

System	Components
1[a]	$p+, p-, +, -$
2[b]	$p+, p-, +$ (or $-$)
3	$p+, p-, +, -$

[a]Because of symmetry, $\rho_{p+} = \rho_{p-}$ and $\rho_{+} = \rho_{-}$.
[b]In such systems, only one type of small ions exists and its type depends on which PE is in excess.

method in a more recent publication.[48] However, the experimental implications of this 3D phase diagram have not been explored.

The 3D phase diagram contains the complete information on the phase behavior of a concentration-asymmetric polycation and polyanion mixture. There are many potentially interesting experimental systems, corresponding to different intercepts/paths in the phase diagram. In the following, we focus on three representative systems that are directly relevant to experiments: 1. a symmetric polycation and polyanion mixture, 2. an asymmetric polycation and polyanion mixture with one type of small ions, and 3. an asymmetric mixture of polycation and polyanion solutions with both types of small ions. In Table I, we list the charged components in each system. Since the symmetric mixture has been extensively studied in the literature, here we mainly focus on the two asymmetric systems. Nevertheless, we briefly discuss the symmetric case, not only because it can be directly compared with existing theoretical predictions but also because it provides a starting point for investigating the asymmetry effects.

B. System 1—Symmetric polycation and polyanion mixture

The intercept between the binodal surface in Fig. 2 and the diagonal surface $\rho_{p+} = \rho_{p-}$ in the 3D phase diagram yields the binodal curve for a symmetric polycation and polyanion mixture. Three such binodal curves are shown in Fig. 3(a). The abscissa denotes the polycation (or polyanion) concentration, and the ordinate denotes the small cation (or anion) concentration. The tie lines shown by the dashes indicate that the small ion concentration in the PE-poor phase is slightly higher than in its coexisting PE-rich phase, i.e., $\rho_{\pm}^{\mathrm{I}} > \rho_{\pm}^{\mathrm{II}}$. The two-phase region disappears above a critical point at $(\rho_{p+,c}, \rho_{+,c})$. Moreover, the phase-separated region shrinks with decreasing l_B and vanishes at a critical value $l_{B,c} \approx 0.2$. Because of the intrinsic symmetry between oppositely charged components in this system, the Galvani potential Ψ_G is identically zero.

Because of its simplicity, the VO theory has been extensively used to study the phase behavior of symmetric polycation and polyanion mixtures.[16,19,22,23] Different values of the parameters including the PE charge fraction f_c and reduced Bjerrum length l_B are used. For instance, in Refs. 16 and 23, f_c is taken to be equal to or smaller than 0.3 for both PE chains and $l_B \approx 2.123$ is used; in Ref. 22, a much higher charge fraction $f_c = 0.95$ but a much smaller $l_B \approx 0.883$ are used for quantitative fitting with experimental data. In order to quantitatively compare with our LS results, in this study we assume that both types of PEs are fully charged (i.e., $f_c = 1$). In Fig. 3(b), we show the binodals calculated by the VO theory for the same set of l_B values as in Fig. 3(a). We see that both the VO and LS theories predict qualitatively similar binodals. A key difference, however, is the opposite slopes for the tie lines between these two results—the VO theory predicts that the PE-rich phase has a higher small ion concentration ($\phi_{+}^{\mathrm{I}} < \phi_{+}^{\mathrm{II}}$). Related to the opposite slopes is the observation that the critical point from the LS theory lies to the right of the maximum on the binodal curve, while the critical point from the VO theory lies slightly to the left of the maximum. We suspect that this difference arises from the chain connectivity correlation, which is completely ignored in the VO theory. We note that the lower small ion concentration in the PE-rich phase predicted by the LS theory is qualitatively consistent with a PRISM-LS theory study,[33] with an RPA study in a wide parameter space,[26] with a more recent renormalized Gaussian fluctuation theory,[70,71] and with recent experiments.[14,49] Another difference is that at a same l_B, the phase-separated region predicted by the VO theory is much larger (in both the PE concentration and the small ion concentration) than that by the LS theory. This is most likely due to the overestimate of electrostatic correlation in the DH correlation energy used in the VO theory.

The intercepts of the binodal in Fig. 3 with the abscissa correspond to the coexisting concentrations for the

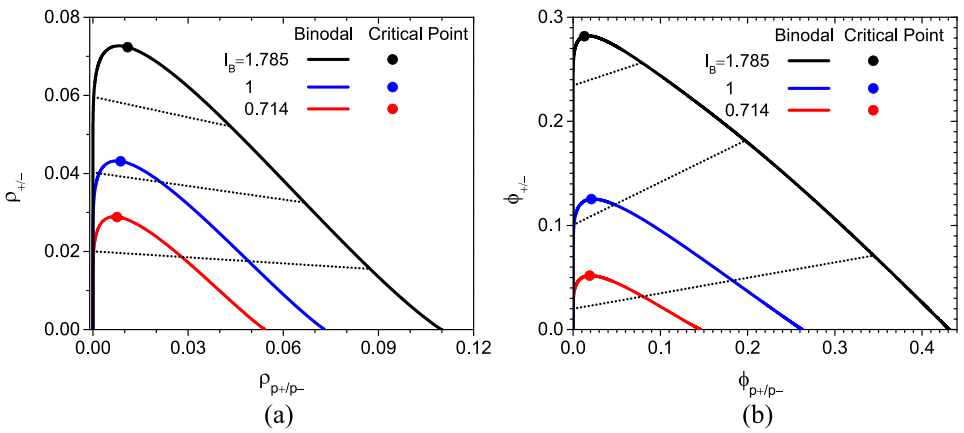

FIG. 3. Phase diagram of *symmetric* polycation and polyanion mixtures with small ions predicted by (a) the liquid-state theory and (b) the Voorn-Overbeek theory. Chain length $N = 100$ is used. The dashed curves represent the tie lines. ϕ in the VO theory can be approximately related to ρ in the LS theory by $\phi = (\pi/6)\rho\sigma^3$.

symmetric mixture *without* small ions. In experiment, such mixtures can be realized by stoichiometrically mixing a polyacid and a symmetric polybase. Ignoring the trace amount of protons (cations) and hydroxyls (anions) due to dissociation of water molecules,[72] the system only contains polycations and polyanions, which act as counterions to each other. In Fig. 4, we show the binodal curves in the ρ_{p+}–l_B phase diagram for such systems with three different values of N. For each N, the phase-separated region lies above the binodal. The critical point, as marked by the solid circle, corresponds to the critical PE concentration $\rho_{p+,c}$ and the critical Bjerrum length $l_{B,c}$. The phase-separated region expands with increasing N due to the decreased translational entropy for both PE chains. For large N, the critical Bjerrum length and the critical concentration follow the scaling behavior $l_{B,c} \sim N^{-1/3}$ and $\rho_{p+,c} \sim N^{-1}$, respectively (data not shown). The exponent −1 is identical to predictions from both VO theory[23] and RPA theory with a fixed Gaussian chain structure;[34] the scaling exponent −1/3, however, is only consistent with that from VO theory but different from that from RPA.[34] Importantly, these scaling relations qualitatively differ from those for the salt-free single-species PE solution (polyanions + small cations), where both $l_{B,c}$ and $\rho_{p+,c}$ are found to be only weakly dependent on N.[52]

C. System 2—Polycation and polyanion mixtures with one type of small ions

1. Phase diagram

The intersection between the coexistence surface and the $\rho_+ = 0$ plane in Fig. 2 results in the binodal curve for a polycation and polyanion mixture with small anions, on the half plane $\rho_{p+} > \rho_{p-}$; the case of $\rho_{p+} < \rho_{p-}$ can be obtained by symmetry. Experimentally, this system can be viewed as a solution of a polycation-polyanion salt plus a PE solution (either polycation or polyanion with its own counterion). Alternatively, we may interpret this system as an asymmetric mixture of a polyacid and a polybase, under the approximation that protons and hydroxyls fully associate into water molecules.[72] For such mixtures, we have three explicit components. Because of charge neutrality, only two of the three components are independent, and we choose the polycation and polyanion as the independent components without loss of generality. While the 3D phase diagram in Fig. 2 only shows the binodal in the half space $\rho_{p+} > \rho_{p-}$, in Fig. 5 we show the full binodal in the polycation–polyanion concentration (ρ_{p+}–ρ_{p-}) phase diagram for such mixtures at l_B = 1.785 (black) and 0.5 (magenta). Because both PEs have the same chain length, all binodals are symmetric with respect to the diagonal. At a given l_B, the phase-separated region lies inside the binodal and the homogeneous region is outside. The tie line (dotted line), connecting compositions in the coexisting phases, is roughly parallel to the diagonal line and shortens with increasing the degree of asymmetry. The critical points ($\rho_{p+,c}$, $\rho_{p-,c}$) are marked by the solid circles. The intersection between the binodal and the diagonal corresponds to the coexisting concentrations ($\rho^{\mathrm{I}}_{p\pm}$, $\rho^{\mathrm{II}}_{p\pm}$) for the fully symmetric mixture without small ions (i.e., Fig. 4). While $\rho^{\mathrm{I}}_{p\pm}$ are usually very small, $\rho^{\mathrm{II}}_{p\pm}$ remain finite and are shown by the open circles. With decreasing l_B, the phase-separated region decreases and disappears at $l_{B,c} \approx 0.2$.

2. Titration of a polyacid with a polybase

While there are several possible experimental implementations for system 2, in the following, we interpret it as a mixture of a polyacid with a polybase since such systems are most commonly studied in experiments.[38,42] On the basis of the binodal in Fig. 5, we predict the titration behavior of a polyacid with a polybase. For simplicity and clarity, we assume both initial solutions have the same PE concentration $\rho_{p,0}$. After mixing volume V_1 of polybase with volume V_2 of polyacid, the overall polycation ($p+$) and polyanion ($p-$) concentrations in the final mixture are $\bar{\rho}_{p+} = (1 + r)\rho_{p,0}/2$ and $\bar{\rho}_{p-} = (1 - r)\rho_{p,0}/2$, respectively, where we remind the readers of the definition of the asymmetry factor $r \equiv (V_1 - V_2)/(V_1 + V_2)$. When $r > 0$ ($r < 0$), the polybase (polyacid) is in excess and thus the small ions are anions (cations) with an overall concentration $\bar{\rho}_{-(+)} = |r|\rho_{p,0}$. Experimentally, increasing r from −1 to 1 corresponds to the gradual titration of a polyacid with a polybase. In the phase diagram shown in Fig. 5, this corresponds to a path that starts on the ordinate and ends on the abscissa in a direction perpendicular to the diagonal line. Differentiating by relative location with respect to the critical point ($\rho_{p+,c}$, $\rho_{p-,c}$), we expect two scenarios of

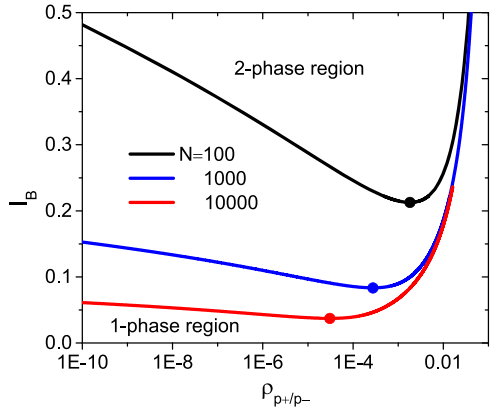

FIG. 4. Binodal curves for the symmetric polycation and polyanion mixture without small ions for different chain lengths. The solid circles denote the critical points.

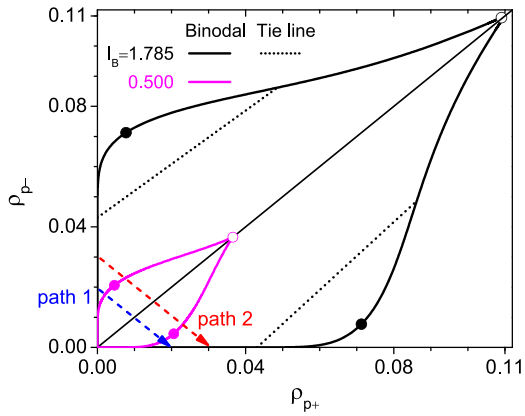

FIG. 5. Phase diagram of a salt-free concentration-asymmetric polyacid and polybase mixture with N = 100. The solid circles denote the critical points.

phase-separation behaviors. In the following, taking the binodal at $l_B = 0.5$ (the magenta curve in Fig. 5) as an example, we examine the evolution of the phase behavior along two typical paths (shown by the dashed arrows in Fig. 5). Along each path, the mixture will undergo phase separation once it enters the phase-separated region, with the concentrations of the coexisting phases determined by the lever rule $\bar{\rho}_i = x\rho_i^{\mathrm{I}} + (1-x)\rho_i^{\mathrm{II}}$ where x is the volume fraction of the PE-poor phase.

In Fig. 6(a), we show the evolution of the volume fraction of the PE-poor phase, x, along these two paths. Due to the symmetry of the binodal, x is symmetric with respect to $r = 0$. For the path with $\rho_{p,0} = 0.02$ (upper curve), with increasing r from -1, x starts to decrease from unity at some finite $-r_1^*$, indicating the emergence of the *PE-rich phase* from the homogeneous solution. The volume fraction of this phase, $1 - x$, grows as r increases towards zero, i.e., as the mixture becomes less asymmetric. At $r = 0$, the polyacid is completely neutralized by the polybase. With further addition of the polybase, the process is reversed, i.e., the volume fraction of the PE-rich phase decreases until this phase disappears at r_1^*. For the path with $\rho_{p,0} = 0.03$ (lower curve), with increasing r, x starts to increase from 0 at some $-r_2^*$, suggesting that now it is the *PE-poor phase* that emerges from the homogeneous solution. The volume fraction of the PE-poor phase x increases monotonically up to the neutralization point $r = 0$. With further increasing r, x decreases monotonically and becomes 0 at r_2^*. These two different scenarios reflect the location of the two paths with respect to the critical point. Moreover, the fact that $r_2^* < r_1^*$ indicates that the amount of polybase required to cause the phase separation is *larger* for systems with higher $\rho_{p,0}$. For sufficiently large $\rho_{p,0}$, no phase separation is possible at any mixing ratio.

While x can exhibit two distinct behaviors along the two different titrating paths, the concentrations of each component in the coexisting phases show qualitatively similar behaviors for the different paths. In Sec. II of the supplementary material, taking the titrating path 1 in Fig. 5 as an example, we illustrate the concentration evolution for each component in the coexisting phases.

The Galvani potential Ψ_G, defined as the electric potential difference between the PE-rich phase and its coexisting PE-poor phase, is uniquely determined by the concentration of each component in both phases. While Ψ_G is exactly 0 for the symmetric mixture, it is generally finite for asymmetric mixtures. Along a specified titrating path, Ψ_G exhibits inversion symmetry, i.e., $\Psi_G(-r) = -\Psi_G(r)$, as shown in Fig. 6(b), so we only discuss the behavior for $r \geq 0$, taking the $\rho_{p,0} = 0.02$ path as an example. First, Ψ_G is positive for $r > 0$, meaning that the PE-rich phase has a higher electric potential. In other words, Ψ_G takes the same sign as the major PE chain. This is consistent with the result from the early VO study.[16] Second, Ψ_G has a sharp peak at $|r| \approx 10^{-3}$. On the scale of the plot in Fig. 6(b), these peaks appear nearly as a discontinuity across $r = 0$. On closer examination, in the narrow region from $r = 0$ to the peak, Ψ_G exhibits two different scaling behaviors: when $r \lesssim 10^{-9}$, $\Psi_G \propto r$ (this is difficult to see on the scale of the figure), as expected from the symmetry property of Ψ_G and its analyticity near $r = 0$. In the range $10^{-9} \lesssim r \lesssim 10^{-3}$, $\Psi_G \sim \ln r$ [note the linear-log scale in the inset of Fig. 6(b)]. We note that Ψ_G is inversely proportional to N (see below). With increasing l_B, the location of the peak shifts to smaller r but the magnitude increases significantly; the boundary differentiating the two distinct scaling regions also shift leftwards.

To understand the behavior of Ψ_G, we return to the phase equilibrium condition $\mu_i^{\mathrm{I}} = \mu_i^{\mathrm{II}} + z_i\Psi_D$. After re-writting μ_i as a sum of an ideal part and an excess part, we have $\rho_i^{\mathrm{I}}/\rho_i^{\mathrm{II}} = \exp\left[N_i\left(\mu_{i,ex}^{\mathrm{II}} - \mu_{i,ex}^{\mathrm{I}} + z_i\Psi_G\right)\right]$. Applying this expression to both PE components and taking the ratio between the two resulting equations, we get

$$\Psi_G = \frac{1}{2N}\ln\left(\frac{\rho_{p+}^{\mathrm{I}}/\rho_{p-}^{\mathrm{I}}}{\rho_{p+}^{\mathrm{II}}/\rho_{p-}^{\mathrm{II}}}\right) + \frac{1}{2}\left[(\mu_{p+,\mathrm{ex}}^{\mathrm{I}} - \mu_{p-,\mathrm{ex}}^{\mathrm{I}}) - (\mu_{p+,\mathrm{ex}}^{\mathrm{II}} - \mu_{p-,\mathrm{ex}}^{\mathrm{II}})\right]. \quad (8)$$

For the symmetric mixture, $\rho_{p+}^{\mathrm{I}} = \rho_{p-}^{\mathrm{I}}$, $\rho_{p+}^{\mathrm{II}} = \rho_{p-}^{\mathrm{II}}$, $\mu_{p+,\mathrm{ex}}^{\mathrm{I}} = \mu_{p-,\mathrm{ex}}^{\mathrm{I}}$, and $\mu_{p+,\mathrm{ex}}^{\mathrm{II}} = \mu_{p-,\mathrm{ex}}^{\mathrm{II}}$, so obviously $\Psi_G = 0$. For an asymmetric mixture, in the PE-rich phase, $\rho_{p+}^{\mathrm{II}}/\rho_{p-}^{\mathrm{II}} \sim O(1)$ and $\mu_{p+,\mathrm{ex}}^{\mathrm{II}} \approx \mu_{p-,\mathrm{ex}}^{\mathrm{II}}$ to a first approximation; in the PE-poor phase, both $\rho_{p\pm}^{\mathrm{I}}$ are small and thus $\mu_{p+,\mathrm{ex}}^{\mathrm{I}} \approx \mu_{p-,\mathrm{ex}}^{\mathrm{I}} \approx 0$. We thus have $\Psi_G \approx \ln(\rho_{p+}^{\mathrm{I}}/\rho_{p-}^{\mathrm{I}})/2N$. When $r > 0$, ρ_{p+}^{I} is larger than ρ_{p-}^{I} and this directly leads to $\Psi_G > 0$. In particular, the sharp peak in Ψ_G for weakly asymmetric mixtures with r slightly larger than 0 is a reflection of $\rho_{p+}^{\mathrm{I}}/\rho_{p-}^{\mathrm{I}} \gg 1$, a consequence of the extreme dilution of the polyanions in phase I and the partition of the added polycations in that phase (which, although

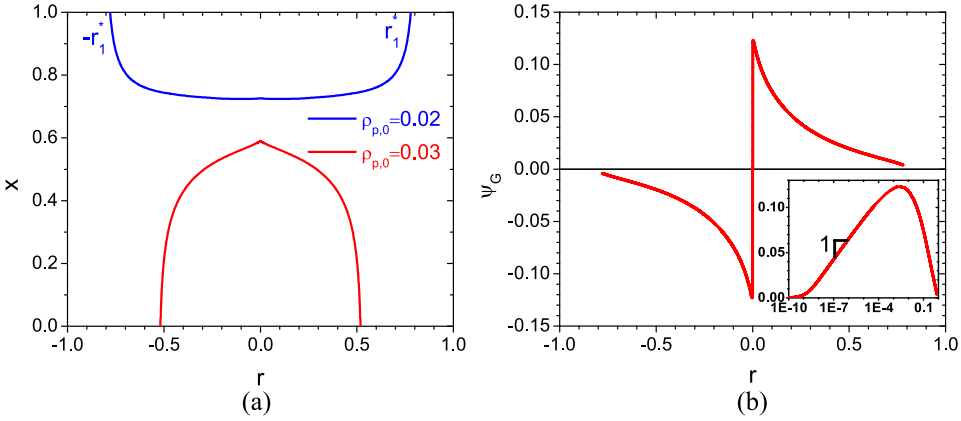

FIG. 6. (a) Volume fraction of the PE-poor phase x vs. the asymmetry factor r along the two titrating paths specified in Fig. 5; (b) The Galvani potential Ψ_G vs. r along the titrating path with $\rho_{p,0} = 0.02$; the inset shows the linear-log plot. $l_B = 0.5$ for all cases.

small in absolute quantity, can increase the polycation concentration by many orders of magnitude). For example, when $r = 0.0023$, $\rho^{\mathrm{I}}_{p+}/\rho^{\mathrm{I}}_{p-}$ is as large as 10^{10}. The scaling behavior for very small r can be understood as follows: when $r \lesssim 10^{-9}$, we can expand ρ^{I}_{p+} and ρ^{I}_{p-} around the symmetry point $r = 0$ as $\rho^{\mathrm{I}}_{p+} \approx c + a_1 r$ and $\rho^{\mathrm{I}}_{p-} \approx c - b_1 r$, respectively, where c is the polycation (polyanion) concentration for the symmetric mixture and $a_1 > 0$ and $b_1 > 0$ are two constants. Thus, $\Psi_D \propto r$. For $10^{-9} \lesssim r \lesssim 10^{-3}$, we still have $\rho^{\mathrm{I}}_{p+} = c + a_1 r \approx a_1 r$, but ρ^{I}_{p-} decreases with added polycation solution as a result of the partition of the small anions into phase I. From Fig. 1(b) of the supplementary material, we find $\rho^{\mathrm{I}}_{p-} \approx b_2/r$. Thus $\Psi_G \approx \ln(a_1 r^2/b_2)/2N \approx (\ln r)/N + \ln(a_1/b_2)/2N$, as observed in the inset of Fig. 6(b). For larger r (in this case $r \gtrsim 10^{-3}$), ρ^{I}_{p-} increases with further addition of polycations—some of the polyanions are transferred from phase II to phase I, and this increase is faster than ρ^{I}_{p+} (see also Fig. 1(b) of the supplementary material); Ψ_G thus starts to decrease monotonically with r. While both $\rho^{\mathrm{I}}_{p\pm}$ are usually too small to be observed accurately in experiments, Ψ_G is sufficiently large to be accurately measured.[74,75]

To briefly summarize the above discussions, the behavior of an asymmetric mixture with $r > 0$ can be understood as follows. In the initial solution (with $r = 0$), there are no small ions and $\rho^{\mathrm{I}}_{p+} = \rho^{\mathrm{I}}_{p-} \approx 0$. Adding some extra polybase brings in the small counter anions which tend to distribute uniformly in the coexisting phases for the sake of translational entropy, i.e., $\rho^{\mathrm{I}}_{-} \approx \rho^{\mathrm{II}}_{-}$. To maintain charge neutrality in the PE-poor phase, there must be approximately the same amount of extra polycations partitioned in this phase, i.e., $\rho^{\mathrm{I}}_{p+} \approx \rho^{\mathrm{I}}_{-}$. When the added concentration of the polycations is less or comparable to the PE concentration in the supernatant phase (phase I), the effect is a small perturbation, resulting in the linear behavior of Ψ_G with r. With a significant (relative to the supernatant concentration) amount of polybase added to the mixture, the added polycations are primarily partitioned into the PE-poor phase, while the polyanions in this phase is further depleted due to displacement by the small anions, leading to the logarithmic regime in Ψ_G vs. r. This directly leads to a huge ratio between ρ^{I}_{p+} and ρ^{I}_{p-} and then a large Ψ_G. However, with further addition of polybase, most of the added polybase goes into phase I. On the other hand, its accompanying anions tend to distribute nearly evenly between the two phases; therefore polyanions are transferred from phase II to phase I to maintain charge neutrality. With a sufficiently large r, the degree of phase-separation weakens until the system enters the homogeneous state.

D. System 3—Asymmetric polycation and polyanion mixtures with both types of small ions

We now consider the asymmetric mixture depicted in Sec. I, where both initial PE solutions have the same PE concentration $\rho_{p,0}$, coion concentration $\rho_{s,0}$, and counterion concentration $\rho_{p,0} + \rho_{s,0}$, where the subscript s in $\rho_{s,0}$ is for "salt" since we envision the coions to be due to added salt (extra salt). After mixing volume V_1 of the polycation solution with volume V_2 of the polyanion solution, the total volume of the mixture is $V = V_1 + V_2$ and the overall concentrations of polycation, polyanion, cation, and anion are, respectively, $\bar{\rho}_{p+} = (1 + r)\rho_{p,0}/2$, $\bar{\rho}_{p-} = (1 - r)\rho_{p,0}/2$, $\bar{\rho}_{+} = (1 - r)\rho_{p,0}/2 + \rho_{s,0}$, and $\bar{\rho}_{-} = (1 + r)\rho_{p,0}/2 + \rho_{s,0}$, where the asymmetry factor $r \equiv (V_1 - V_2)/V$ again characterizes the degree of asymmetry of the mixture. When $r = 0$, the mixture reduces to system 1 discussed in Sec. III B, while the case $r = 1$ (or -1) corresponds to a pure polycation (or polyanion) solution, which we studied in Ref. 52. For the general case, the final mixture is globally characterized by three parameters—r, $\rho_{s,0}$, and $\rho_{p,0}$. When the point $(\bar{\rho}_{p+}, \bar{\rho}_{p-}, \bar{\rho}_{+})$, which is specified by the parameter set (r, $\rho_{s,0}$, $\rho_{p,0}$)—falls within the phase-separated region of Fig. 2, the system will phase-separate into a PE-poor phase and a PE-rich phase, with the volume fraction of each phase and the concentrations of each component in the coexisting phases determined by the lever rule

$$\bar{\rho}_i = x\rho^{\mathrm{I}}_i + (1 - x)\rho^{\mathrm{II}}_i, \tag{9}$$

where again we use x to refer to the volume fraction of the PE-poor phase. While the phase diagram is given in terms of the overall concentrations $(\bar{\rho}_{p+}, \bar{\rho}_{p-}, \bar{\rho}_{+})$, experimentally the more easily controllable parameters are the asymmetry factor r, the extra salt concentration $\rho_{s,0}$, and the initial PE concentration $\rho_{p,0}$. Therefore, in the following, we will examine the effects of these parameters in turn, on the phase behavior of an *asymmetric* polycation and polyanion mixture with both types of small ions.

1. Effect of the asymmetric factor r

First we study the effect of the asymmetry factor r for mixtures at fixed $\rho_{p,0}$ and $\rho_{s,0}$. Physically, varying r corresponds to varying the mixing ratio between the two initial solutions. Because the compositions in both initial solutions are symmetric, the behavior for the mixture (r, $\rho_{p,0}$, $\rho_{s,0}$) is identical with the mixture ($-r$, $\rho_{p,0}$, $\rho_{s,0}$), with the role of anions and cations exchanged. We thus only discuss the case $r \in [0, 1]$, where the polycation is the major PE species and the anion is the major small ion. Since the solution with $r = 0$ denotes a symmetric mixture (i.e., system 1), the solution with $r > 0$ can be interpreted as adding extra polycation and small anion solution into the initially symmetric mixture. We now examine how the extra polycations and anions partition in the coexisting phases and how their addition affects the phase behavior of the initial mixture.

Without extra salt. We first consider the mixture without extra salt (i.e., $\rho_{s,0} = 0$) at fixed $\rho_{p,0}$. In Fig. 7(a), we show the volume fraction of the PE-poor phase x as a function of the asymmetry factor r for four different values of $\rho_{p,0}$ (e.g., $\rho_{p,0} = 0.006$, 0.04, 0.07 and 0.08). Note that for all four systems, the mixtures are phase separated at $r = 0$. For the three lower values of $\rho_{p,0}$, as extra polycation solution is added to the system, x first decreases slightly at small $r \in [0, 0.02]$, but tends to increase at large r and becomes unity at some special r^*, where the PE-rich phase disappears. On the other hand, for the larger $\rho_{p,0} = 0.08$, x decreases monotonically and becomes 0 at another r^*, meaning it is the PE-poor phase that vanishes. Physically, r^* quantifies the boundary mixing ratio beyond which the system enters the single-phase state. Taking $\rho_{p,0} = 0.08$ as an example,

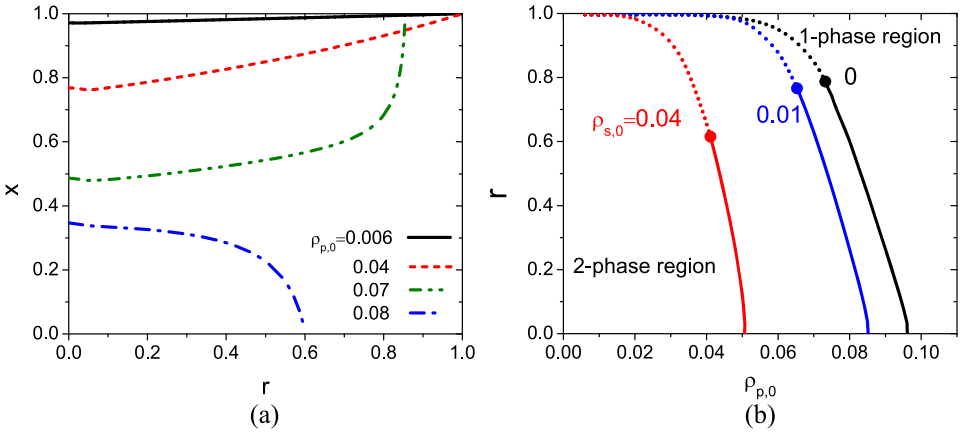

FIG. 7. (a) Volume fraction of the PE-poor phase x vs. the asymmetry factor r in the range $r \in [0, 1]$ for the mixtures without extra salt at different initial PE concentration $\rho_{p,0}$. (b) Phase diagram in the $\rho_{p,0}-r$ plane for mixtures at different $\rho_{s,0}$; see the main text for details.

$r^* \approx 0.6$ indicating that, when the volume ratio between the initial solutions is either larger than 4: 1 or smaller than 1: 4, the mixture is in a homogeneous state; otherwise, the mixture undergoes a phase separation. Moreover, for systems with small $\rho_{p,0}$ (e.g., 0.006 and 0.04), r^* is very close to 1, implying that phase-separation can still take place even for highly asymmetric mixtures if both initial solutions are sufficiently dilute. Viewed in another way, addition of a small amount of polyanion solution into a pure polycation solution can induce phase separation, when both solutions are dilute (but still denser than the supernatant concentration in a phase-separated system, which is usually exceedingly dilute). With increasing $\rho_{p,0}$, r^* decreases monotonically, signifying the shrinkage of the phase-separated region along r. In Fig. 7(b), we show the r^* vs. $\rho_{p,0}$ phase diagram; the black curve is for the case without extra salt. The dotted and solid segments, respectively, represent that it is the PE-rich phase and the PE-poor phase that vanishes at r^*; the black circle is a critical point differentiating these two segments. Clearly, the single-phase region corresponds to higher initial PE concentration $\rho_{p,0}$ and/or the larger asymmetric parameter r.

Accompanying the evolution of the volume fraction, the concentration of each component in the two phases also adjusts to satisfy mass conservation, Eq. (9). We recall that for the mixture without extra salt, increasing r corresponds to adding a polycation solution. Therefore, the overall polycation and anion concentrations increase linearly with r ($\bar{\rho}_{p+} = \bar{\rho}_{-} = (1+r)\rho_{p,0}/2$), while the overall polyanion and cation concentrations decrease linearly ($\bar{\rho}_{p-} = \bar{\rho}_{+} = (1-r)\rho_{p,0}/2$). Taking $\rho_{p,0} = 0.006$ as an example, in Fig. 8(a) we show, respectively, the concentration for the polycation (blue) and for the polyanion (red) in the *PE-poor* phase $\rho^{\mathrm{I}}_{p\pm}$ as a function of r.

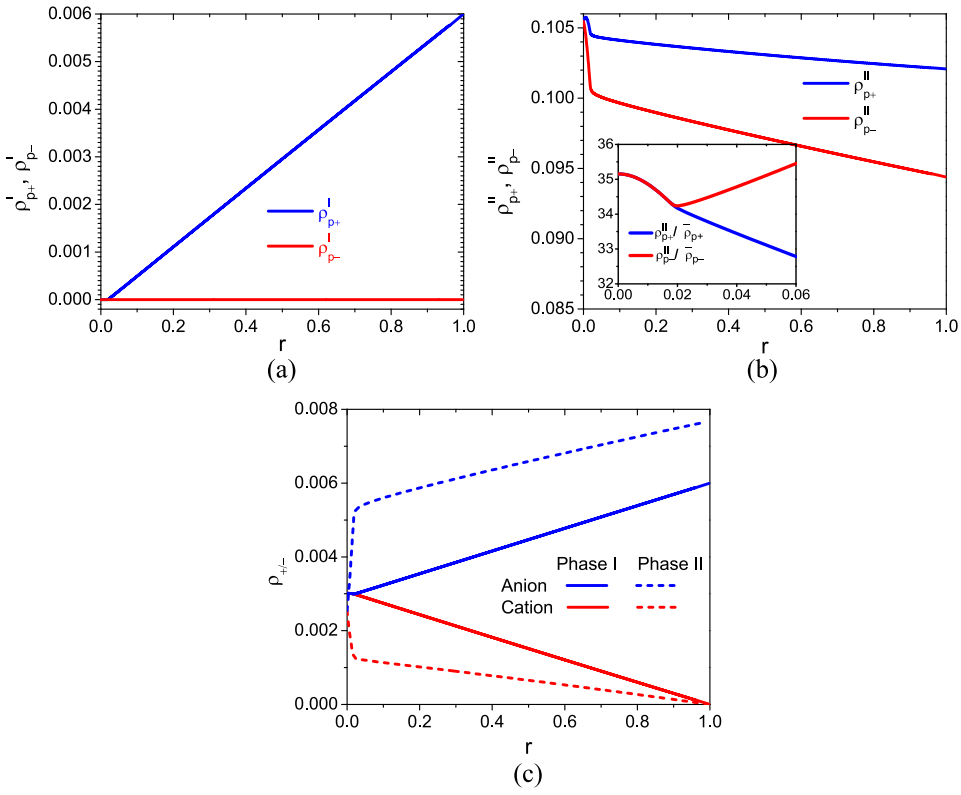

FIG. 8. Polycation and polyanion concentrations (a) in the PE-poor phase, $\rho^{\mathrm{I}}_{p\pm}$, and (b) in the PE-rich phase, $\rho^{\mathrm{II}}_{p\pm}$, vs. the asymmetry factor $r \in [0, 1]$. Inset of part (b) shows the ratio $\rho^{\mathrm{II}}_{p\pm}/\bar{\rho}_{p\pm}$. (c) Small ion concentrations in both phases $\rho^{\mathrm{I/II}}_{\pm}$ vs. $r \in [0, 1]$. All three figures are for the system without extra salt and at fixed $\rho_{p,0} = 0.006$. It is worth noting that all curves terminate at r^*, whose value for the chosen set of parameters is very close to but not equal to 1.

First, we see that ρ^{I}_{p-} remains very close to 0 in the entire phase-separated region, i.e., there are very few minor PEs in the PE-poor phase. A log-log plot actually shows that ρ^{I}_{p-} exhibits a minimum at some r (data not shown), indicating that increasing r will initially make the PE-poor phase even more depleted of the minor PE chain. The polycation concentration in this phase ρ^{I}_{p+}, however, exhibits two distinct regimes. For $r \lesssim 0.02$, $\rho^{\mathrm{I}}_{p+} \approx 0$ (due to the exceedingly low PE concentration in the supernatant phase), signifying that initially nearly all the added polycations (the major PE component) go to the PE-poor phase (and dragging some polyanion chains away from the PE-poor phase). For $0.02 \lesssim r < r^*$, $\rho^{\mathrm{I}}_{p+} \approx r\rho_{p,0}$ and approaches $\rho_{p,0}$ at r^* (where the PE-rich phase disappears). The above results suggest that, for weakly asymmetric mixtures, the concentration of both PEs in the PE-poor phase is very low. For slightly more asymmetric mixtures, while the minor PE concentration remains very low in the PE-poor phase, adding the major PE species (in this case the polycation) results in an appreciable amount of this species in this phase. Furthermore, while both $\rho^{\mathrm{I}}_{p\pm}$ for weakly asymmetric mixtures ($0 < r \ll r^*$) are too small to be accurately measured in experiments, the ratio between them can be very large which results in a large Galvani potential Ψ_G (see the results later).

Next, in Fig. 8(b), we show both PE concentrations in the *PE-rich* phase $\rho^{\mathrm{II}}_{p\pm}$. Because both the polycation and polyanion concentrations are exceedingly low in the PE-poor phase, before a significant amount of the added major PE goes to the dilute phase, by Eq. (9), we have $\rho^{\mathrm{II}}_{p\pm} \approx \bar{\rho}_{p\pm}/(1-x)$. Therefore, in this regime, the PE concentration is determined primarily by the overall $\bar{\rho}_{p\pm}$ and the volume fraction of the PE-rich phase $1-x$. Since $\bar{\rho}_{p+} = \bar{\rho}_{-} = (1+r)\rho_{p,0}/2$, the initial decrease in ρ^{II}_{p+} is caused by the initial slight increase in the volume fraction of the PE-rich phase with r. (With a different initial $\rho_{p,0}$, the increase in the volume fraction of the PE-rich phase can be slower than the increase in $\bar{\rho}_{p+}$, leading to a slight *increase* in ρ^{II}_{p+}). On the other hand, ρ^{II}_{p-} can only decrease in this regime since the numerator $\bar{\rho}_{p-}$ decreases with r, while the denominator $1-x$ increases with r. Moreover, since in this regime, $\rho^{\mathrm{II}}_{p\pm} \approx \bar{\rho}_{p\pm}/(1-x)$, we have $\rho^{\mathrm{II}}_{p+}/\bar{\rho}_{p+} \approx \rho^{\mathrm{II}}_{p-}/\bar{\rho}_{p-}$ [see the inset of Fig. 8(b)].

For $0.02 \lesssim r < r^*$, we enter the regime where a significant amount of the added polycations are partitioned into the PE-poor phase, so the first term in the right-hand side of the lever rule Eq. (9) for the polycations can no longer be ignored. The resulting ρ^{II}_{p+} can either decrease [as shown in Fig. 8(b)] or increase (data not shown), depending on the initial PE concentration $\rho_{p,0}$. The magnitude of the change, however, is small (a few percent) in the entire range of r for all the cases we have examined. On the other hand, for the polyanions, $x\rho^{\mathrm{I}}_{p-}$ remains negligible in most cases (except near the critical region); therefore, $\rho^{\mathrm{II}}_{p-} \approx \bar{\rho}_{p-}/(1-x)$ decreases, mainly because of the decrease of $\bar{\rho}_{p-}$ with r. We remark that, ρ^{II}_{p-} remains finite in the entire range of the two-phase region; it is only the amount of the PE-rich phase that decreases and eventually disappears at the phase boundary r^* whose value is very close to 1 for the set of chosen parameters in the figure.

For the symmetric mixtures, the LS theory predicts that in most cases, the small ions have slightly higher concentration in the PE-poor phase [see Fig. 3(a)]. In particular, for the system with $\rho_{p,0} = 0.006$ and $\rho_{s,0} = 0$ specified here, $\rho^{\mathrm{I}}_{+} = \rho^{\mathrm{I}}_{-} = 0.003\,01$ and $\rho^{\mathrm{II}}_{+} = \rho^{\mathrm{II}}_{-} = 0.002\,54$. For the asymmetric mixtures, however, the situation is quite different. In Fig. 8(c), we show cation and anion concentrations in the coexisting phases $\rho^{\mathrm{I/II}}_{\pm}$ as a function of the asymmetric factor r. Because $\bar{\rho}_{-}$ increases with r, the anion concentration in both phases, $\rho^{\mathrm{I/II}}_{-}$, goes up with r. Likewise, the cation concentration in both phases, $\rho^{\mathrm{I/II}}_{+}$, decreases with r, following the behavior of $\bar{\rho}_{+}$. Moreover, except for very small r, the cation concentration in the PE-poor phase is larger than that in the PE-rich phase, i.e., $\rho^{\mathrm{I}}_{+} > \rho^{\mathrm{II}}_{+}$, while the opposite trend is observed for the anion $\rho^{\mathrm{I}}_{-} < \rho^{\mathrm{II}}_{-}$; this is qualitatively different from the symmetric mixture. Furthermore, similar to PE concentrations, $\rho^{\mathrm{I/II}}_{\pm}$ likewise exhibit different behaviors in two r regimes. (1) For $0 \le r \lesssim 0.02$, since the polycation and polyanion concentrations in the PE-poor phase are nearly zero, $\rho^{\mathrm{I}}_{+} \approx \rho^{\mathrm{I}}_{-}$ to maintain charge neutrality, and both are roughly independent of r (see the solid red and black curves at small r). In the PE-rich phase, however, ρ^{II}_{+} (the red dashed curve) decreases abruptly, while ρ^{II}_{-} increases rapidly; this rapid variation is strongly related to the fact that nearly all extra polycations are partitioned into the PE-rich phase in this r regime. Although one might expect that the extra anions should also go predominantly to the PE-rich phase to maintain charge neutrality, such a partition is disfavored by the translational entropy of anions. This translational entropy drives a significant fraction of the added anions into the PE-poor phase, with the accompanying transfer of cations from the PE-rich phase into the PE-poor phase to maintain charge neutrality. (2) For $0.02 \lesssim r < r^*$, since the PE-poor phase occupies most of the system volume (i.e., x is very close to 1), we have $\rho^{\mathrm{I}}_{-} \approx \rho_{p,0}(1+r)/2$ (the blue solid line) and $\rho^{\mathrm{I}}_{+} \approx \rho_{p,0}(1-r)/2$ (the red solid line). For the PE-rich phase, both $\rho^{\mathrm{II}}_{\pm}$ change almost linearly with r, with the increase in ρ^{II}_{+} outpacing the decrease in ρ^{II}_{-}.

From the above discussion, we conclude the following physical picture on the partition of the added polycations and small anions in the coexisting phases. For very weak asymmetry (i.e., $0 < r \lesssim 0.02$, corresponding to adding only a small amount of polycation solution), the added polycations tend to accumulate in the PE-rich phase to lower the electrostatic energy. The extra anions, however, are partitioned in both phases and some cations in the PE-rich phase *transfer* into the PE-poor phase to minimize the translational entropy penalty as well as to maintain charge neutrality in the coexisting phases. While this partition results in increased concentration differences for both the cations and anions between the coexisting phases, the gain in the overall electrostatic energy is still large enough to lower the total free energy. This scenario is schematically shown in Fig. 9(a). For the asymmetric mixtures with $0.02 < r < r^*$, however, the gain in the electrostatic energy can no longer compensate for the loss in the translational entropy for the small ions if the extra polycations stay predominantly in the PE-rich phase, and consequently, these extra polycations and anions are distributed in both phases in a way such that the overall free energy is minimized. Figure 9(b)

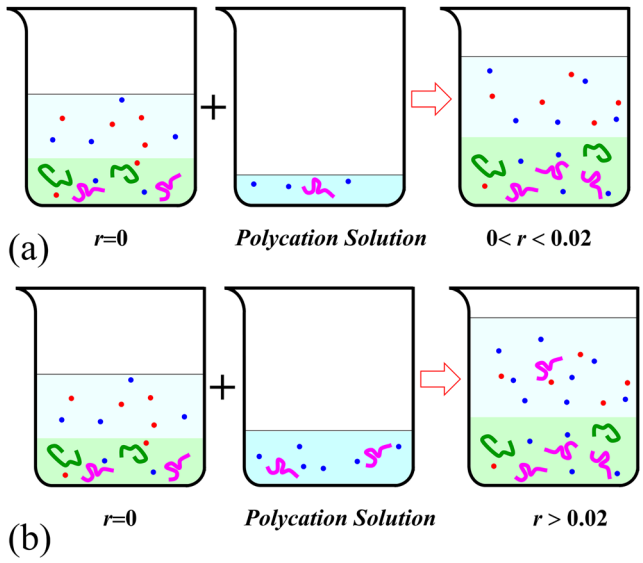

FIG. 9. Schematics for the partition of the newly added polycation solutions in the initially symmetric mixture, part (a) is for a small amount of extra polycation solution and part (b) is for a large amount of extra polycation solution.

schematically shows the partition of extra components for such mixtures.

Our discussion on the partition of the components in the coexisting phases has been based on a particular value of the initial PE concentration $\rho_{p,0} = 0.006$. For other values of $\rho_{p,0}$, the evolution of the volume fraction can be completely different [see the black and the blue curves in Fig. 7(a), for example]. However, the concentrations of the different components in the coexisting phases exhibit overall qualitatively similar behaviors, and we thus do not show the data here. In Sec. III of the supplementary material, we briefly discuss some of the main differences, taking the case with $\rho_{p,0} = 0.08$ as an example.

Next, we discuss the Galvani potential Ψ_G vs. r for the mixture without extra salt with $\rho_{p,0} = 0.006$. First, we note Ψ_G has the inversion symmetry $\Psi_G(-r) = -\Psi_G(r)$ and Ψ_G has the same sign as r in the entire phase-separated regime. For the $r > 0$ cases we have been discussing in this section, this again means that the PE-rich phase always has a higher electric potential since polycations are the major PE species. Second, Ψ_G exhibits sharp peaks around $|r| = 0.02$. This maximum is again strongly related to the huge concentration asymmetry between the major PE and minor PE species in the PE-poor phase, similar to the behavior observed in Fig. 6(b) for system 2. Third, at small r, Ψ_G is approximately proportional to r, and it can be rationalized by similar argument as for system 2. However, since now there are two small-ion species, the depletion of the minor PE species from the PE-poor phase is not as substantial as in system 2, and consequently we do not find the logarithm scaling relation observed there.

With extra salt. For asymmetric mixtures with finite $\rho_{s,0}$, the evolution of the phase behavior (the volume fraction of each phase and the concentration of the different ion species in each phase) along r is discussed in Sec. IV of the supplementary material. In particular, we find that the phase-separation window along r shrinks for systems with finite $\rho_{s,0}$. In Fig. 7(b), we summarize the phase diagram in r^* vs. $\rho_{p,0}$ for systems with $\rho_{s,0} = 0.01$ and 0.04 (the blue and red curves), respectively, in analogy to the extra-salt–free case (the black curve). It is obvious that the phase-separation region becomes narrower for mixtures with larger $\rho_{s,0}$. With increasing $\rho_{s,0}$, the two different regimes along r observed for the salt-free case shown in Fig. 8 become less distinct and become indistinguishable for sufficiently large $\rho_{s,0}$. Correspondingly, the blue curve in Fig. 10 shows that the peaks in Ψ_G become much weaker and shift to larger values of $|r|$ for systems with finite $\rho_{s,0}$.

2. Effect of extra-salt concentration $\rho_{s,0}$

It is well-known that salt plays an important role in determining phase behaviors of PE solutions; a prominent example is the salting-out and salting-in phenomena.[51,52,73] Experimentally, increasing the extra-salt concentration $\rho_{s,0}$ can be simply achieved by adding pure salt into an initial mixture. For an asymmetric polycation and polyanion mixture at fixed r and $\rho_{p,0}$, with increasing $\rho_{s,0}$, the degree of phase separation always becomes weaker and the system enters the single-phase region at the salting-in point $\rho^*_{s,0}$. This is qualitatively different from a single PE solution with salt,[52] where adding salt initially broadens the miscibility gap. Moreover, for a mixture with smaller $\rho_{p,0}$ or larger $|r|$, it is the PE-rich phase that is "salted-in", while for mixtures with smaller r or larger $\rho_{p,0}$, it is the PE-poor phase that is "salted-in." Following the same procedure used in constructing the $\rho_{p,0}-r$ phase diagram (in Fig. 7), we likewise construct the phase boundary in the $\rho_{s,0}-r$ phase diagram, as shown by Fig. 11. For each $\rho_{p,0}$, the phase-separated region lies below the phase boundary and the single-phase region is above it. Again, the solid and the dotted curve/segment, respectively, represent the phase boundary at which the PE-poor phase and the PE-rich phase vanish. It is obvious that the phase-separated region shrinks with larger $\rho_{p,0}$.

We now examine the effect of $\rho_{s,0}$ on the concentration of each component in the coexisting phases. First we note that the overall concentrations of both PEs $\bar{\rho}_{p\pm}$ remain invariant with $\rho_{s,0}$. Taking the mixture with $\rho_{p,0} = 0.006$ as an example, Fig. 12(a) shows that both PE concentrations

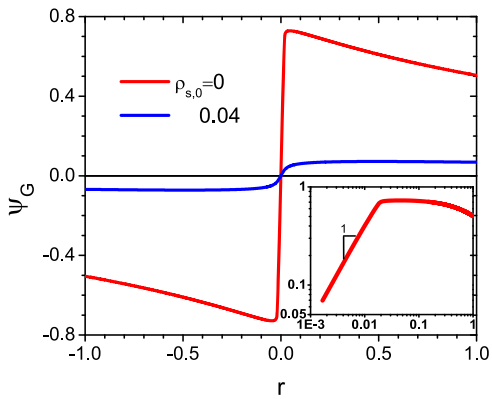

FIG. 10. Galvani potential Ψ_G vs. the asymmetric factor r for the mixture with $\rho_{p,0} = 0.006$. Inset shows the log-log plot of the behavior for $r > 0$.

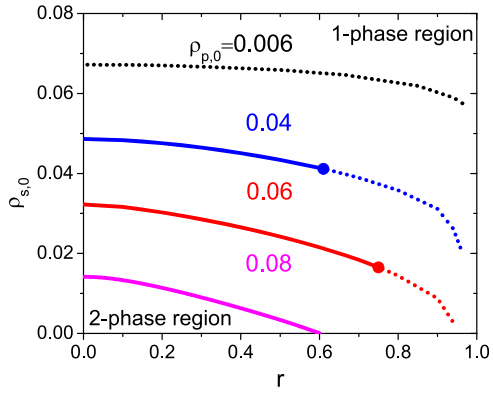

FIG. 11. Phase diagram in the $r-\rho_{s,0}$ plane for mixtures at several values of $\rho_{p,0}$. The dotted and the solid curve/segment means the vanishing phase is the PE-rich phase and PE-poor phase, respectively.

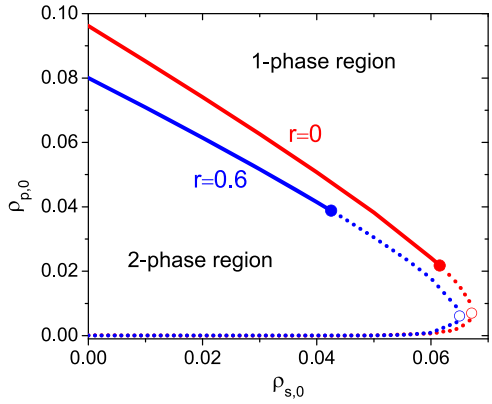

FIG. 13. Phase diagram in the $\rho_{s,0}-\rho_{p,0}$ plane at fixed r; see the main text for details.

in the PE-poor phase $\rho^{\mathrm{I}}_{p\pm}$ exhibit two different behaviors. In a wide range of $\rho_{s,0}$, for the symmetric case (the black curve), both $\rho^{\mathrm{I}}_{p\pm} \approx 0$, indicating that the PE-poor phase is very dilute in both PEs. For asymmetric mixtures (the blue and red curves), while the minor PE concentration $\rho^{\mathrm{I}}_{p-} \approx 0$, the major PE concentration ρ^{I}_{p+} remains nearly constant and its value is larger for the more asymmetric mixtures. Since the volume of the PE-poor phase in this regime decreases with $\rho_{s,0}$ (data not shown), the constant ρ^{I}_{p+} implies that adding salt drives some major PEs (polycations for $r > 0$) to move from the PE-poor phase to the PE-rich phase. As $\rho_{s,0}$ approaches the phase boundary, both $\rho^{\mathrm{I}}_{p\pm}$ increase rapidly with $\rho_{s,0}$; this indicates that there is a significant amount of both PEs transferring from the PE-rich phase back to the PE-poor phase.

In contrast to the behavior of the PE concentrations in the PE-poor phase, Fig. 12(b) shows that both PE concentrations in the PE-rich phase $\rho^{\mathrm{II}}_{p\pm}$ decrease monotonically with $\rho_{s,0}$. The initial decrease is primarily due to the increase in the volume of the PE-rich phase, while for $\rho_{s,0}$ close to the phase boundary, the decrease of $\rho^{\mathrm{I/II}}_{p\pm}$ is again mainly due to the transfer of both PE chains to the PE-poor phase. In addition, we find that, at a given $\rho_{s,0}$, the PE concentrations ($\rho^{\mathrm{II}}_{p\pm}$) are nearly independent of r although the minor PE concentration (ρ^{II}_{p-}) is slightly smaller for the more asymmetric system. For the small ions, for the asymmetric mixture, the concentration of the minor ion species is always higher in the PE-poor phase, but the concentration of the major ion species is higher in the PE-rich phase at small $\rho_{s,0}$ and is higher in the other phase at large $\rho_{s,0}$ (data not shown). Finally, the Galvani potential Ψ_G decreases monotonically with $\rho_{s,0}$ for a mixture at fixed $r > 0$ and $\rho_{p,0}$ (data not shown).

3. Effect of initial PE concentration $\rho_{p,0}$

In this section, we turn to examine how the initial PE concentration $\rho_{p,0}$ affects the phase behavior of an asymmetric mixture. Experimentally, decreasing $\rho_{p,0}$ at fixed r and $\rho_{s,0}$ corresponds to diluting the mixture with a simple electrolyte solution with the same $\rho_{s,0}$. Generally, for a mixture at fixed r and $\rho_{s,0}$, phase-separation only occurs in the range of $\rho^{*}_{p,0} < \rho_{p,0} < \rho^{**}_{p,0}$, where $\rho^{*}_{p,0}$ and $\rho^{**}_{p,0}$, respectively, denote the lower and the upper boundaries of this range. (We emphasize that these values are not to be confused with the coexisting concentrations of the PE-poor and PE-rich phases since $\rho_{p,0}$ refers to the *initial* PE concentration.) With increasing $\rho_{p,0}$, the volume fraction of the PE-poor phase x decreases from 1 at $\rho^{*}_{p,0}$, i.e., it is the PE-rich phase that emerges; on the other hand, except for mixtures with large $\rho_{s,0}$, generally x decreases to 0 at $\rho^{**}_{p,0}$, implying that it is mostly the PE-poor phase that vanishes upon increasing $\rho_{p,0}$. Moreover, $\rho^{*}_{p,0}$ is very close to 0 except for the cases with large $\rho_{s,0}$, i.e., phase separation usually occurs even for very dilute mixtures. In Fig. 13, we show $\rho^{*}_{p,0}$ and $\rho^{**}_{p,0}$ in the $\rho_{s,0}-\rho_{p,0}$ phase diagram. For each r, the phase-separated region lies inside the

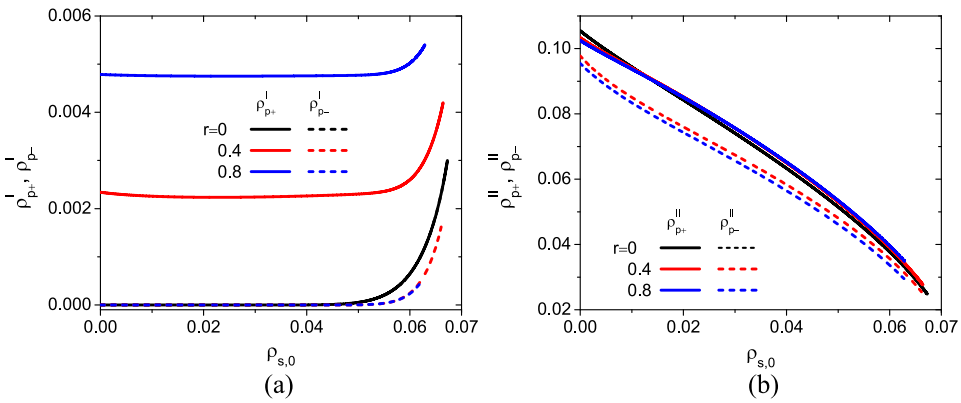

FIG. 12. Polycation and polyanion concentrations (a) in the PE-poor phase, $\rho^{\mathrm{I}}_{p\pm}$, and (b) in the PE-rich phase, $\rho^{\mathrm{II}}_{p\pm}$ vs. the extra-salt concentration $\rho_{s,0}$ for both symmetric and asymmetric mixtures with $\rho_{p,0} = 0.006$. The black solid and dashed curves in both figures overlap due to the symmetry of the mixtures.

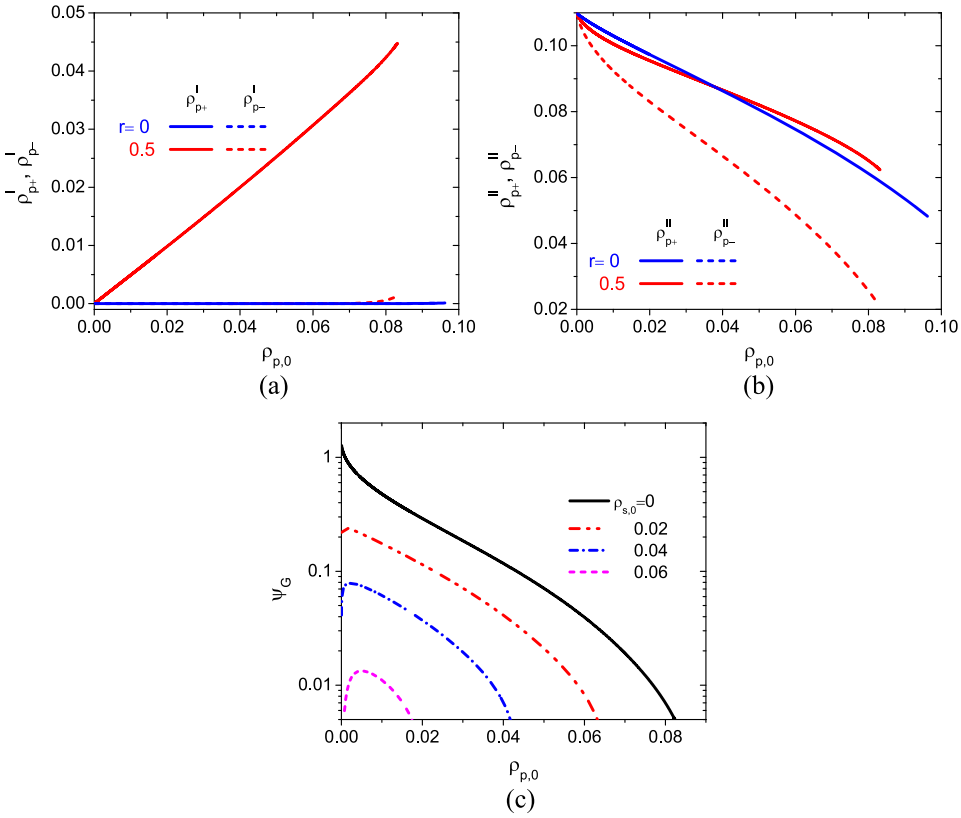

FIG. 14. Polycation and polyanion concentrations (a) in the PE-poor phase, $\rho^{\mathrm{I}}_{p\pm}$ and (b) in the PE-rich phase, $\rho^{\mathrm{II}}_{p\pm}$ vs. the initial PE concentration $\rho_{p,0}$ for mixtures with $\rho_{s,0} = 0$. The blue solid and dashed curves in (a) and (b) overlap due to the symmetry of the mixtures. (c) Galvani potential Ψ_G vs. $\rho_{p,0}$ for the asymmetric systems with $r = 0.5$ and different $\rho_{s,0}$.

curve, while the homogeneous one-phase region outside. Each curve consists of two branches—the lower branch denotes $\rho^{*}_{p,0}$ and the upper branch represents $\rho^{**}_{p,0}$. With increasing $\rho_{s,0}$, these two branches approach each other and merge at a special point marked by the open circle. Moreover, the upper branch of $\rho^{**}_{p,0}$ consists of two segments; the solid and dotted segments, respectively, represent the cases where the vanishing phases are the PE-poor phase and the PE-rich phase, and the solid circle denotes the critical point differentiating these two segments. It is obvious that the phase-separated region in the $\rho_{s,0}-\rho_{p,0}$ phase diagram becomes narrower for the more asymmetric system.

In Figs. 14(a) and 14(b), we show the PE concentrations in the PE-poor phase $\rho^{\mathrm{I}}_{p\pm}$ and in the PE-rich phase $\rho^{\mathrm{II}}_{p\pm}$, respectively. First we recall that, at fixed r and $\rho_{s,0}$, the overall concentration for both PE species increases linearly with $\rho_{p,0}$, i.e., $\bar{\rho}_{p+} = r\rho_{p,0}$ and $\bar{\rho}_{p-} = (1-r)\rho_{p,0}$. From Fig. 14(a), we see that, for the symmetric mixture, both $\rho^{\mathrm{I}}_{p\pm} \approx 0$ in the entire phase-separated region. For the asymmetric mixture, only the minor PE concentration is close to 0, while the major PE concentration increases approximately linearly with $\rho_{p,0}$. On the other hand, Fig. 14(b) shows that both $\rho^{\mathrm{II}}_{p\pm}$ decrease monotonically, in spite of the linear increase in the overall $\bar{\rho}_{p\pm}$ with $\rho_{p,0}$. This seeming paradox can be rationalized by noticing that the volume fraction of the PE-rich phase increases with $\rho_{p,0}$. Moreover, ρ^{II}_{p+} (the major PE species) is weakly dependent on r, consistent with the observation in Fig. 8(b). For the small ion concentrations, for an asymmetric mixture with $r > 0$, the minor small ion (cation) concentration is always higher in PE-poor phase, but the major small ion concentration in the PE-rich phase has a non-monotonic behavior: it is higher (than in the PE-poor phase) when $\rho_{p,0}$ is very small and r is large, and it is lower when $\rho_{p,0}$ is large or r is small. Finally, Fig. 14(c) shows the Galvani potential Ψ_G vs. $\rho_{p,0}$ for the asymmetric mixture ($r = 0.5$) with different $\rho_{s,0}$. For $\rho_{s,0} = 0$, Ψ_G decreases monotonically with $\rho_{p,0}$; for mixtures with finite $\rho_{s,0}$, however, Ψ_G exhibits a maximum at some $\rho_{p,0}$ where $\rho^{\mathrm{I}}_{p+}/\rho^{\mathrm{I}}_{p-}$ approximately reaches a peak. In addition, at given $\rho_{p,0}$, Ψ_G decreases with $\rho_{s,0}$ because of the weaker degree of phase-separation.

IV. SUMMARY AND CONCLUSIONS

Using a simple liquid state (LS) theory, we have systematically studied the phase behaviors of a *concentration-asymmetric* mixture of polycation and polyanion solutions, taking the simplest case where both polycation and polyanion have the same chain length and are fully charged, and all charged species are monovalent. A three-dimensional (3D) polycation–polyanion–cation concentration ($\rho_{p+}-\rho_{p-}-\rho_{+}$) phase diagram at a fixed Bjerrum length l_B has been constructed. This phase diagram contains the complete phase behavior information at the specified l_B and yields rich and complex phase-separation scenarios that are directly relevant to experiments. As Sec. III has given a detailed exposition of the results, here we briefly recapitulate the main findings of our work, in ascending order of complexity of the system specification: a symmetric polycation and polyanion mixture, an asymmetric mixture with one type of small ions, and an asymmetric mixture with both types of small ions.

For the symmetric mixture, the LS theory predicts that small ion concentration is higher in the PE-poor phase under most conditions; this is consistent with previous theoretical

work using PRISM-LS,[33] RPA,[26,27] and a renormalized Gaussian fluctuation theory[71] and with recent experiments,[14,49] but is in stark contrast to the VO theory calculation,[16,23] which predicts small ion enrichment in the PE-rich phase under all conditions.

The binodal of the asymmetric mixture with one type of small ions corresponds to the intercept between the 2D binodal surface of the 3D phase diagram and the bottom surface (i.e., $\rho_+ = 0$), and one possible experimental interpretation (realization) is the titration of a polyacid with a symmetric polybase. We predict two different scenarios of phase separation, according to the evolution in the volume fraction of each phase along the titrating path, i.e., whether it is the PE-rich or PE-poor phase that first appear or disappear. Moreover, we find that the Galvani potential Ψ_G—the electrostatic potential difference between the PE-rich phase and its coexisting PE-poor phase—exhibits two sharp peaks of opposite sign on either side of the symmetry point, giving the appearance of a nearly discontinuous jump between these two peaks across the point of symmetry; these sharp peaks arise from the very large disparity between polycation and polyanion concentrations in the PE-poor phase near the symmetry point. While the concentrations of different species (especially in the PE-poor phase) may be difficult to measure accurately in experiments, both the volume fraction of each phase and the Galvani potential Ψ_G can be readily and accurately determined.[74,75]

For asymmetric mixtures with both types of small ions, we have re-expressed the information in the three-dimensional $\rho_{p+}-\rho_{p-}-\rho_+$ phase diagram by relating to the experimentally more easily controllable parameters: the asymmetry factor r, the extra-salt concentration $\rho_{s,0}$, and the initial PE concentrations $\rho_{p,0}$. For any fixed two of the three parameters, we have calculated the evolution in the volume fraction of each phase and the variation of the concentrations of each charged species in the coexisting phases with the third parameter. Importantly, we have constructed three $\rho_{p,0}-r$, $r-\rho_{s,0}$, and $\rho_{s,0}-\rho_{p,0}$ phase diagrams [see Figs. 7(b), 11, and 13, respectively]; compared with the original 3D phase diagram, these phase diagram represent a simple means to experimentally determine the general phase behavior in coacervate systems in the easy-to-control set of variables r, $\rho_{s,0}$, and $\rho_{p,0}$. In particular, we find that for systems with small $\rho_{p,0}$ and $\rho_{s,0}$, a minute amount of polycation solution into a polyanion solution can lead to phase separation, and the phase separation window along r shrinks with increasing $\rho_{p,0}$ or $\rho_{s,0}$ and vanishes for sufficiently large $\rho_{p,0}$ or $\rho_{s,0}$. Similar to that in the titration of a polyacid with a symmetric polybase, the Galvani potential Ψ_G[74,75] also exhibits two peaks near the symmetry point whose sharpness decreases with increasing salt concentration.

For asymmetric mixtures (say $r > 0$ for definiteness) without extra salts or with small $\rho_{s,0}$, we find two distinct r regimes for the partition of added PEs (polycations) and small ions in the coexisting phases: starting from the symmetric mixture, upon adding a small amount of polycation solution, the added polycations are partitioned almost entirely in the PE-rich phase, due to the gain in the electrostatic correlation energy; the extra small anions, however, are partitioned in both phases, and some cations in the PE-rich phase transfer into the PE-poor phase to maintain charge neutrality [see Fig. 9(a)]. With further addition of polycation solutions into the mixture, a substantial amount of extra polycations goes to the PE-poor phase [see Fig. 9(b)], largely driven by the translational entropy of the anions (in combination with the charge neutrality requirement).

Additionally, we find that the minor PE concentration in the PE-poor phase remains close to 0 under all conditions except near the critical line; the major PE concentration in this phase, however, is nearly independent of the extra-salt concentration $\rho_{s,0}$ but increases approximately linearly with the initial PE concentration $\rho_{p,0}$ and the asymmetry factor r. In the PE-rich phase, on the other hand, both PE concentrations are only weakly dependent on the asymmetric factor r but decreases monotonically with increasing $\rho_{s,0}$ and $\rho_{p,0}$. We expect all these predictions to be observed in experiments. Indeed, for the symmetric mixture, recent experiment by Li *et al.*[14] has shown the decrease of the PE concentration in the PE-rich phase with increasing initial PE concentration $\rho_{p,0}$.

We end this article by making the following remarks. First, in this work, we have only focused on effects of the simplest asymmetry, i.e., the concentration-asymmetry, on the phase behaviors of oppositely charged PE mixtures. Even for this simplest case, our study reveals a wealth of interesting and complex phase separations scenarios. Asymmetry in other parameters, including chain length, charge fraction, sizes of PE segment and small ions, and small ion valency, should play a significant role and further enrich the phase behavior.[22,38–45] Studies of their effects along similar lines to this work will provide the theoretical basis for controlling the system behavior by tuning these parameters. Second, while the present LS theory qualitatively captures the main physics governing the phase behavior in the coacervate-forming systems, several important effects, for example, solvent quality effects and strong electrostatic correlation effects (including the counterion condensation effect[76] and pairing between oppositely charged PEs in the dilute phase[32]). Incorporation of these effects will lead to quantitative improvements in the predicted results; see Refs. 32, 34, 35, 48, and 71 for recent advances in this direction. However, we expect the qualitative features elucidated in our study to remain valid. Third, our study has only examined the simple two-phase coexistence; at stronger electrostatic strengths, multiple-phase coexistence may exist. For example, the PE-poor phase for the asymmetric mixture, which mainly consists of three charged components (the major PE component, coion, and counterion—thus corresponding to the system studied in Ref. 52) may further undergo another liquid-liquid phase separation at sufficiently large l_B. We will pursue this possibility in the future. Finally, the bulk phase behaviors examined in the work can serve as a starting point for investigation of inhomogeneous systems, such as the interfacial tension of the coacervate phase and PE layer-by-layer assembly, using the classical density functional theory.[77]

SUPPLEMENTARY MATERIAL

See supplementary material for the methods for constructing the phase diagrams, and it contains additional results

supporting the discussions in the main text. In Sec. I, we present two different approaches to calculating the phase diagrams for the four-component systems studied in this paper. In Sec. II, we examine the evolution in the concentration of the various species for a titrating path in a polycation and polyanion mixture with one type of small ions. In Sec. III, we study the effect of the asymmetry factor r for mixtures without extra salt at large $\rho_{p,0}$ and highlight the difference with the otherwise same system at small $\rho_{p,0}$ examined in the main text. Finally, in Sec. IV, we show results of the effect of r on the phase behavior for mixtures with finite $\rho_{s,0}$.

ACKNOWLEDGMENTS

This work was conducted jointly by King Fahd University of Petroleum and Minerals (KFUPM), Dhahran, Saudi Arabia and California Institute of Technology (Caltech) under a collaborative research program in catalysis. The authors gratefully acknowledge the support provided by KFUPM and Caltech. J.W. acknowledges partial financial support from the U.S. National Science Foundation (Grant No. NSF-CBET-8200852353).

[1] G. Decher, Science **277**, 1232 (1997).
[2] J. Borges and J. F. Mano, Chem. Rev. **114**, 8883 (2014).
[3] K. A. Black, D. Priftis, S. L. Perry, J. Yip, W. Y. Byun, and M. Tirrell, ACS Macro Lett. **3**, 1088 (2014).
[4] D. W. Pan and M. E. Davis, Bioconjugate Chem. **26**, 1791 (2015).
[5] Q. Zhao, D. W. Lee, B. K. Ahn, S. Seo, Y. Kaufman, J. N. Israelachvili, and J. H. Waite, Nat. Mater. **15**, 407 (2016).
[6] B. P. Lee, P. B. Messersmith, J. N. Israelachvili, and J. H. Waite, Annu. Rev. Mater. Res. **41**, 99 (2011).
[7] R. J. Stewart, T. C. Ransom, and V. Hlady, J. Polym. Sci., Part B: Polym. Phys. **49**, 757 (2011).
[8] B. Philipp, H. Dautzenberg, K. J. Linow, J. Kötz, and W. Dawydoff, Prog. Polym. Sci. **14**, 91 (1989).
[9] A. F. Thünemann, M. Müller, H. Dautzenberg, J.-F. Joanny, and H. Löwen, Adv. Polym. Sci. **166**, 113 (2004).
[10] J. van der Gucht, E. Spruijt, M. Lemmers, and M. A. Cohen Stuart, J. Colloid Interface Sci. **361**, 407 (2011).
[11] A. Veis, Adv. Colloid Interface Sci. **167**, 2 (2011).
[12] C. E. Sing, Adv. Colloid Interface Sci. **239**, 2 (2017).
[13] S. Srivastava and M. V. Tirrell, Adv. Chem. Phys. **161**, 499 (2016).
[14] L. Li, S. Srivastava, M. Andreev, A. Marciel, J. J. de Pablo, and M. Tirrell, Macromolecules **51**, 2988 (2018).
[15] M. Voorn, Recl. Trav. Chim. Pays-Bas **75**, 317 (1956).
[16] J. Overbeek and M. Voorn, J. Cell. Comp. Physiol. **49**, 7 (1957).
[17] P. Debye and E. Hückel, Phys. Z **24**, 185 (1923).
[18] M. Voorn, Recl. Trav. Chim. Pays-Bas **75**, 405 (1956).
[19] M. Voorn, Recl. Trav. Chim. Pays-Bas **75**, 427 (1956).
[20] M. Voorn, Recl. Trav. Chim. Pays-Bas **75**, 925 (1956).
[21] M. Voorn, Recl. Trav. Chim. Pays-Bas **75**, 1021 (1956).
[22] E. Spruijt, A. H. Westphal, J. W. Borst, M. A. Cohen Stuart, and J. van der Gucht, Macromolecules **43**, 6476 (2010).
[23] J. Qin, D. Priftis, R. Farina, S. Perry, L. Leon, J. Whitmer, K. Hoffmann, M. Tirrell, and J. J. de Pablo, ACS Macro Lett. **3**, 565 (2014).
[24] A. Veis, J. Phys. Chem. **65**, 1798 (1961).
[25] M. Castelnovo and J.-F. Joanny, Eur. Phys. J. E **6**, 377 (2001).
[26] A. Kudlay and M. O. de la Cruz, J. Chem. Phys. **120**, 404 (2004).
[27] A. Kudlay, A. V. Ermoshkin, and M. O. de la Cruz, Macromolecules **37**, 9231 (2004).
[28] P. M. Biesheuvel and M. A. C. Stuart, Langmuir **20**, 2785 (2004).
[29] P. M. Biesheuvel and M. A. C. Stuart, Langmuir **20**, 4764 (2004).
[30] P. K. Jha, P. S. Desai, J. Li, and R. G. Larson, Polymers **6**, 1414 (2014).
[31] J. Lee, Y. O. Popov, and G. H. Fredrickson, J. Chem. Phys. **128**, 224908 (2008).
[32] K. T. Delaney and G. H. Fredrickson, J. Chem. Phys. **146**, 224902 (2017).
[33] S. L. Perry and C. E. Sing, Macromolecules **48**, 5040 (2015).
[34] J. Qin and J. J. de Pablo, Macromolecules **49**, 8789 (2016).
[35] A. Salehi and R. G. Larson, Macromolecules **49**, 9706 (2016).
[36] A. M. Rumyantseva and I. I. Potemkin, Phys. Chem. Chem. Phys. **19**, 27580 (2017).
[37] R. Zhang and B. I. Shklovskii, Phys. A **352**, 216 (2005).
[38] R. Chollakup, W. Smitthipong, C. D. Eisenbach, and M. Tirrell, Macromolecules **43**, 2518 (2010).
[39] J. Wang, M. A. Cohen Stuart, and J. van der Gucht, Macromolecules **45**, 8903 (2012).
[40] Q. Wang and J. B. Schlenoff, Macromolecules **47**, 3108 (2014).
[41] A. Salehi, P. S. Desai, J. Li, C. A. Steele, and R. G. Larson, Macromolecules **48**, 400 (2015).
[42] D. Priftis and M. Tirrell, Soft Matter **8**, 9396 (2012).
[43] S. Perry, Y. Li, D. Priftis, L. Leon, and M. Tirrell, Polymers **6**, 1756 (2014).
[44] A. B. Kayitmazer, A. F. Koksal, and E. K. Iyilik, Soft Matter **11**, 8605 (2015).
[45] A. C. Obermeyer, C. E. Mills, X.-H. Dong, R. J. Flores, and B. D. Olsen, Soft Matter **12**, 3570 (2016).
[46] N. N. Oskolkov and I. I. Potemkin, Macromolecules **40**, 8423 (2007).
[47] M. Zhao, J. Zhou, C. Su, L. Niu, D. Liang, and B. Li, J. Chem. Phys. **142**, 204902 (2015).
[48] T. K. Lytle and C. E. Sing, Soft Matter **13**, 7001 (2017).
[49] M. Radhakrishna, K. Basu, Y. Liu, R. Shamsi, S. L. Perry, and C. E. Sing, Macromolecules **50**, 3030 (2017).
[50] L. Chang, T. K. Lytle, M. Radhakrishna, J. J. Madinya, J. Vélez, C. E. Sing, and S. L. Perry, Nat. Commun. **8**, 1273 (2017).
[51] H. Eisenberg and G. R. Mohan, J. Phys. Chem. **63**, 671 (1959).
[52] P. Zhang, N. M. Alsaifi, J. Wu, and Z.-G. Wang, Macromolecules **49**, 9720 (2016).
[53] J. Jiang, H. Liu, Y. Hu, and J. M. Prausnitz, J. Chem. Phys. **108**, 780 (1998).
[54] J. Jiang, L. Blum, O. Bernard, and J. Prausnitz, Mol. Phys. **99**, 1121 (2001).
[55] M. Wertheim, J. Stat. Phys. **35**, 19 (1984).
[56] M. Wertheim, J. Stat. Phys. **35**, 35 (1984).
[57] M. Wertheim, J. Chem. Phys. **87**, 7323 (1987).
[58] T. Boublík, J. Chem. Phys. **53**, 471 (1970).
[59] G. A. Mansoori, N. F. Carnahan, K. E. Starling, and T. W. Leland, Jr., J. Chem. Phys. **54**, 1523 (1971).
[60] N. F. Carnahan and K. E. Starling, J. Chem. Phys. **51**, 635 (1969).
[61] J.-P. Hansen and I. R. McDonald, *Theory of Simple Liquids*, 4th ed. (Academic Press, London, 2013).
[62] E. Waisman and J. Lebowitz, J. Chem. Phys. **56**, 3086 (1972).
[63] E. Waisman and J. Lebowitz, J. Chem. Phys. **56**, 3093 (1972).
[64] L. Blum, Mol. Phys. **30**, 1529 (1975).
[65] K. Hiroike, Mol. Phys. **33**, 1195 (1977).
[66] H. Anderson and D. Chandler, J. Chem. Phys. **57**, 1918 (1972).
[67] H. Anderson, D. Chandler, and J. Weeks, J. Chem. Phys. **57**, 2626 (1972).
[68] The first line of Eq. (7) in our previous publication[52] has a typographic error: the denominator $4(1-\eta)$ in the second term in the brackets should be $4(1-\eta)^2$. The correct equation was used in our calculations, however.
[69] I. Mills, T.Cvitaš, K. Homann, N. Kallay, and K. Kuchitsu, *Green Book, IUPAC Quantities, Units and Symbols in Physical Chemistry*, 2nd ed. (Blackwell Scientific Publications, Oxford, 1993), p. 59.
[70] K. Shen and Z.-G. Wang, J. Chem. Phys. **146**, 084901 (2017).
[71] K. Shen and Z.-G. Wang, Macromolecules **51**, 1706 (2018).
[72] Strictly speaking, the concentrations of hydroxyl OH^- (anion) and hydrogen ion H^+ (cation) are governed by the equilibrium constant $[H^+] \cdot [OH^-] = K_w(M^2)$, with $K_w = 10^{-14}$ for pure water at room temperature. For a symmetric mixture, the concentrations of both small ions can be neglected; likewise, for an asymmetric mixture, the concentration of one of the two small ions can be approximately taken to be 0 (System 3). For a more sophisticated treatment explicitly including chemical equilibrium between H^+ and OH^-, see Ref. 35 for a recent development. As a second remark, in experiments, both polyacid and polybase chains can be either weakly or strongly charged, depending on the pH. In this work, we assume both PEs to be fully charged for simplicity.
[73] N. Volk, D. Vollmer, M. Schmidt, W. Oppermann, and K. Huber, Adv. Polym. Sci. **166**, 29 (2004).
[74] M. Vis, V. Peters, R. Tromp, and R. Erné, Langmuir **30**, 5755 (2014).
[75] H. Jensen, V. Devaud, J. Josserand, and H. H. Girault, J. Electroanal. Chem. **537**, 77 (2002).
[76] G. S. Manning, J. Chem. Phys. **51**, 924 (1969).
[77] Z. Li and J. Wu, Phys. Rev. Lett. **96**, 048302 (2006).